Akt inhibition promotes autophagy and sensitizes PTEN-null tumors to lysosomotropic agents

Michael Degtyarev,[1] Ann De Mazière,[2] Christine Orr,[1] Jie Lin,[1] Brian B. Lee,[1] Janet Y. Tien,[1] Wei W. Prior,[1] Suzanne van Dijk,[2] Hong Wu,[3] Daniel C. Gray,[1] David P. Davis,[1] Howard M. Stern,[1] Lesley J. Murray,[1] Klaus P. Hoeflich,[1] Judith Klumperman,[2] Lori S. Friedman,[1] and Kui Lin[1]

[1]Genentech, Inc., South San Francisco, CA 94080
[2]Cell Microscopy Center, Department of Cell Biology and Institute for Biomembranes, University Medical Center Utrecht, 3584 CX Utrecht, Netherlands
[3]Department of Molecular and Medical Pharmacology, University of California, Los Angeles, Los Angeles, CA 90095

Although Akt is known as a survival kinase, inhibitors of the phosphatidylinositol 3-kinase (PI3K)–Akt pathway do not always induce substantial apoptosis. We show that silencing Akt1 alone, or any combination of Akt isoforms, can suppress the growth of tumors established from phosphatase and tensin homologue–null human cancer cells. Although these findings indicate that Akt is essential for tumor maintenance, most tumors eventually rebound. Akt knockdown or inactivation with small molecule inhibitors did not induce significant apoptosis but rather markedly increased autophagy. Further treatment with the lysosomotropic agent chloroquine caused accumulation of abnormal autophagolysosomes and reactive oxygen species, leading to accelerated cell death in vitro and complete tumor remission in vivo. Cell death was also promoted when Akt inhibition was combined with the vacuolar H^+–adenosine triphosphatase inhibitor bafilomycin A1 or with cathepsin inhibition. These results suggest that blocking lysosomal degradation can be detrimental to cancer cell survival when autophagy is activated, providing rationale for a new therapeutic approach to enhancing the anticancer efficacy of PI3K–Akt pathway inhibition.

Introduction

Aberrant activation of the class I phosphatidylinositol 3-kinase (PI3K)/Akt pathway has been widely implicated in a variety of cancers, and the three Akt isoforms represent attractive cancer therapeutic targets (Samuels and Ericson, 2006; Stambolic and Woodgett, 2006). Genetic ablations of *Akt* genes in mice have revealed both distinct and overlapping functions of each isoform in normal physiology (Chen et al., 2001; Cho et al., 2001a,b; Peng et al., 2003; Easton et al., 2005; Tschopp et al., 2005; Yang et al., 2005) and tumor initiation (Chen et al., 2006; Skeen et al., 2006; Ju et al., 2007; Maroulakou et al., 2007). The relative contribution of the Akt isoforms in maintaining human tumor growth remains elusive, however. Human cancers usually coexpress two or all three Akt isoforms, and amplification or hyperactivation of each isoform has been documented in different types of cancers (Stahl et al., 2004; Altomare and Testa, 2005). Mounting evidence suggests that Akt isoforms may be differentially regulated depending on the external stimuli and the tissue studied and may regulate distinct aspects of cellular processes in a cell- and tissue-specific manner (Kim et al., 2001; Tanno et al., 2001; Dufour et al., 2004; Irie et al., 2005; Samuels et al., 2005; Yoeli-Lerner et al., 2005).

Akt is well known for its antiapoptotic activity when overexpressed under stress conditions (Amaravadi and Thompson, 2005). However, inhibiting components of the PI3K–Akt pathway

C. Orr and J. Lin contributed equally to this paper.

Correspondence to Kui Lin: klin@gene.com

D. Gray's present address is Chemistry and Biology Graduate Program, University of California, San Francisco, San Francisco, CA 94158.

Abbreviations used in this paper: AO, acridine orange; AV, autophagic vacuole; AVO, acidic vesicular organelle; Ba, bafilomycin A1; CCD, charge-coupled device; CQ, chloroquine; Dox, doxycycline; IHC, immunohistochemistry; KD, knockdown; LAMP, lysosome-associated membrane protein; MDC, monodansylcadaverine; MEF, mouse embryonic fibroblast; mTOR, mammalian target of rapamycin; NAC, *N*-acetylcysteine; PARP, poly-ADP-ribose polymerase; PI, propidium iodide; PI3K, phosphatidylinositol 3-kinase; PTEN, phosphatase and tensin homologue; ROS, reactive oxygen species; shAkt, Akt-targeting shRNA; shRNA, short hairpin RNA.

The online version of this article contains supplemental material.

The Rockefeller University Press $30.00
J. Cell Biol. Vol. 183 No. 1 101–116
www.jcb.org/cgi/doi/10.1083/jcb.200801099

often does not induce substantial apoptosis without additional proapoptotic insults. This is exemplified in a recent study where a dual PI3K/mammalian target of rapamycin (mTOR) inhibitor that efficiently inhibited phosphorylation of Akt blocked proliferation of glioma xenografts without the induction of apoptosis (Fan et al., 2006). However, the enhanced tumorigenesis stimulated by a constitutively active Akt is linked to its ability to inhibit autophagy but not apoptosis in a recent study (Degenhardt et al., 2006), raising the possibility that autophagy may also be an important mechanism underlying the response to therapeutic agents targeting the PI3K–Akt pathway. Autophagy is a catabolic process characterized by the appearance of autophagic vacuoles (AVs) in the cytoplasm, leading to self-digestion of cytoplasmic organelles and other constituents in the lysosomal compartments. Although autophagy may be capable of ultimate cell killing when allowed to reach its limit, it is also thought to be a temporary survival mechanism under stress conditions, and inhibiting autophagy can either promote or inhibit cell death depending on the conditions and agents used (Lockshin and Zakeri, 2004; Kroemer and Jaattela, 2005; Levine and Yuan, 2005; Amaravadi et al., 2007).

In this study, we describe the use of inducible short hairpin RNAs (shRNAs) to specifically and stably knock down each of the three individual Akt isoforms, both singly and in all possible combinations, in human cancer cells deficient for the tumor suppressor phosphatase and tensin homologue (PTEN), a negative regulator of the PI3K–Akt pathway. This approach avoids the possible nonspecific or side effects associated with systemic treatment of small molecule inhibitors, allowing us to evaluate the specific contributions of the Akt proteins in proliferation, survival, and tumor maintenance both in vitro and in vivo. We show that silencing Akt1 alone can suppress tumor growth, whereas simultaneous knockdown (KD) of all three isoforms provides the most consistent and pronounced tumor growth inhibition. The tumor cells exhibit markedly increased autophagy as a major response to reduced Akt activity, whereas classical apoptosis was not the prevailing response. Blocking lysosome function by lysosomotropic agents or cathepsin inhibition significantly increased the sensitivity of tumor cells to Akt inhibition both in vitro and in vivo, suggesting a critical role for autolysosomal degradation in cell survival under Akt inhibition.

Results

Inducible shRNA KD of Akt isoforms inhibited the growth of PTEN-null human tumor xenografts in a dose- and isoform-dependent manner

To determine the relative contribution of the three Akt isoforms in maintaining tumor growth, we used a tet-inducible shRNA KD method using a recently described retroviral vector system, pHUSH (a tet-inducible plasmid vector for H1 or U6 short hairpin; Gray et al., 2005; Hoeflich et al., 2006). We chose the PTEN-null human prostate cancer cell line PC3 and the glioma cell line U87MG (Li et al., 1997). Both lines express all three Akt isoforms; in PC3 cells, Akt1 protein is expressed at approximately two times the level of Akt2, with Akt3 contributing to <10% of total Akt, whereas in U87MG cells, all three Akt proteins are expressed at equivalent levels (Fig. S1 A, available at http://www.jcb.org/cgi/content/full/jcb.200801099/DC1). Stable clones of PC3 and U87MG cells were generated harboring inducible shRNA constructs targeting all possible single and combined Akt isoforms (Table S1). Each Akt-targeting shRNA (shAkt) caused ~75–99% KD of the corresponding Akt mRNA and proteins upon doxycycline (Dox) induction (Fig. 1 A, Fig. S1 B, and Table S2). Decreased steady-state phosphorylation of downstream targets PRAS40 and S6, up-regulation of $p27^{Kip1}$, and feedback stabilization of IRS1 were observed to varying degrees in response to the KDs, with the strongest effects observed in cells with all three Akt KDs (Fig. 1 A).

We next examined the effect of Akt KDs on the ability of PC3 cells to maintain the growth of established tumors in vivo. Dox-induced KD of Akt2 (shAkt2) or Akt3 (shAkt3) alone did not result in significant inhibition of tumor growth (Fig. 1 B and Table S2). In contrast, two different shRNA constructs targeting Akt1 (shAkt1) both showed significant tumor growth inhibition, each in two out of three independent clones. Tumor growth retardation or stasis was typically observed in these clones (Fig. 1 B, Fig. S1 H, and Table S2). Simultaneous KD of Akt1,2 (shAkt12) or Akt1,3 (shAkt13) also inhibited tumor growth, with almost all tumor growth halted and tumor regression observed in several of the Dox-treated mice. Interestingly, KD of both Akt2 and Akt3 (shAkt23) also resulted in significant tumor growth inhibition, with no tumor volume doubling during the 2 wk of Dox treatment, suggesting that Akt1 activity alone is not sufficient to maintain optimal tumor growth. Finally, triple-Akt KD (shAkt123) most effectively inhibited tumor growth, with consistent tumor regression observed during the first 2 wk of treatment. Similar results were observed in U87MG cells, which express similar levels of the three Akt isoforms. Among the three single KDs, only shAkt1 showed significant tumor stasis, and tumor regression was again observed with triple-Akt KD (Fig. S1, C–F). Thus, KD of Akt1 alone can inhibit tumor growth in both PC3 and U87MG xenografts, and this Akt1 dependency is not simply a total Akt dose effect. More pronounced tumor growth inhibition and regression, however, occurs in tumors with KD of all three Akt isoforms.

Akt KDs induced cell cycle delay without significant apoptosis

Analysis of PC3 tumors with Akt KDs revealed a mild decrease in the proliferation marker Ki-67 and no significant increase in TUNEL-positive cells compared with control tumors (Fig. 2 A). The lack of apoptosis was also observed in PC3 cells cultured in vitro. Under 10% FBS, a mild increase in G0/G1 and a decrease in S phase was observed in cells expressing each shAkt construct. Slightly increased accumulation of cells in the G2/M phase was also observed in cells expressing shRNA for Akt1 alone and any combinations of two or three Akt isoforms, suggesting a cell cycle delay in both DNA replication and mitosis in these cells. However, no significant sub-G1 population was observed with any of the KDs (Fig. S2, A and B, available at http://www.jcb.org/cgi/content/full/jcb.200801099/DC1). Additional experiments also failed to detect significant caspase

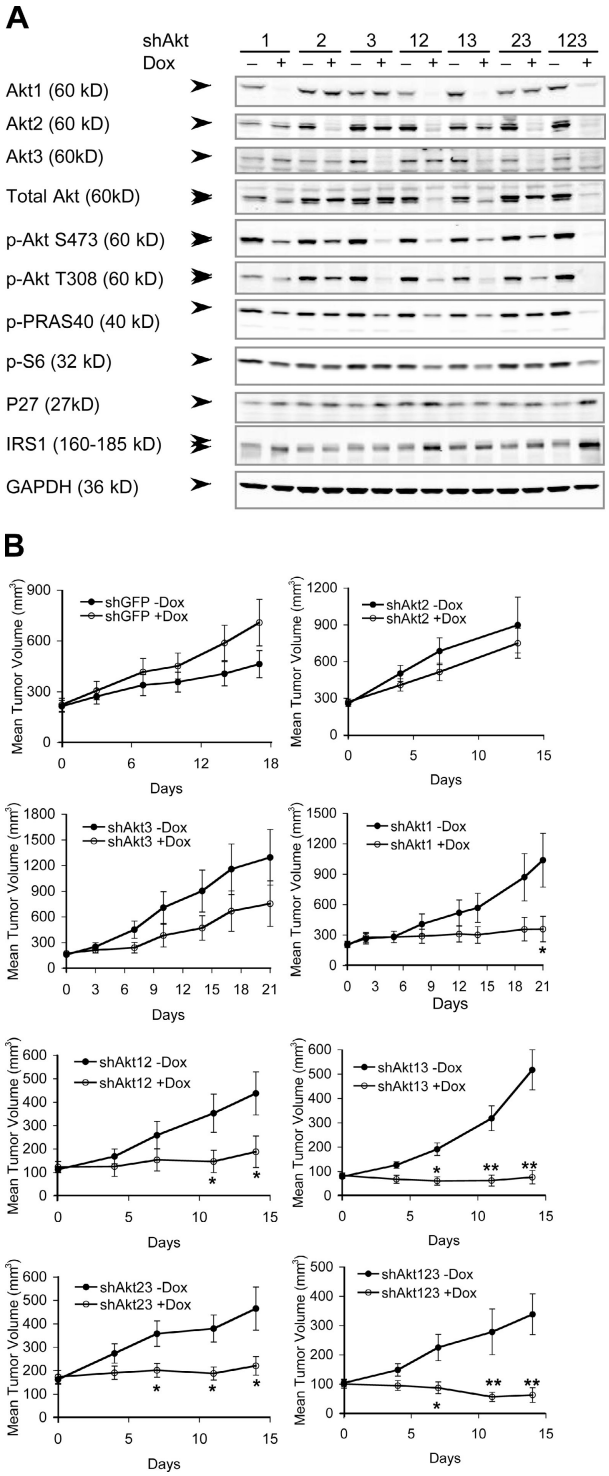

Figure 1. **Inducible KD of Akt isoforms and their effect on xenograft tumor growth.** (A) Immunoblot analysis of Akt isoforms and various downstream proteins in stable PC3 clones expressing the inducible shRNA constructs. Each clone was induced to express the respective shRNAs with 1 µg/ml Dox grown under 10% FBS for 7 d. Double arrowheads indicate slight differences in the mobility of the three Akt isoforms detected by total and phospho-Akt antibodies and the mobility shift of IRS1. (B) Effect of Akt KD on xenograft tumor growth. Representative experiments showing the growth of PC3 xenograft tumors containing the various shRNAs treated with vehicle control (−Dox, closed circles) or Dox (+Dox, open circles; see Table S2, available at http://www.jcb.org/cgi/content/full/jcb.200801099/DC1). Error bars represent SEM. *, $P < 0.05$; **, $P < 0.005$.

activation in response to Akt KDs in both PC3 and U87MG cells (unpublished data). To partially mimic the suboptimal growth condition in the in vivo environment, we starved the cells of serum in culture and asked whether the cells became more sensitive to Akt KD. Indeed, complete serum starvation or reducing serum to 0.5% resulted in markedly increased accumulation of cells in the G0/G1 phase. However, still no significant sub-G1 peak was observed for at least 2 d in 0% FBS and 5 d in 0.5% FBS (Fig. 2, B and C).

Akt KD promoted autophagy in PC3 and U87MG cells

Because Akt has been shown to inhibit autophagy (Arico et al., 2001; Degenhardt et al., 2006), we asked whether specific KD of endogenous Akt could promote autophagy. Indeed, EM analysis revealed a significantly increased accumulation of AVs in both PC3 and U87MG cells induced to express shAkt123 (Fig. 3, A and B; and Fig. S2 C). The accumulation of AV and acidic vesicular organelles (AVOs) was further confirmed by localization of the autophagosome marker GFP-LC3, staining with an anti-LC3 antibody, and fluorescent dyes monodansylcadaverine (MDC) and acridine orange (AO; Fig. 4 A, Fig. S2, D–G, and not depicted).

We examined xenograft tumors expressing shAkt by EM. The control GFP-targeting shRNA–expressing PC3 tumors consist of healthy looking cells connected by cell–cell junctions (Fig. 3 C, a). In contrast, cells in the shAkt123-expressing tumors exhibit morphological signs of degeneration and loss of cell–cell contact after 10–15 d of Dox treatment (Fig. 3 C, b). Late AVs positive for human lysosome-associated membrane protein (LAMP)1 are found in degenerating tumor cells (Fig. 3 C, b–d). Also, these cells often contain swollen mitochondria and dilated RER that are drastically disorganized, suggesting a connection between energy metabolism, ER stress, and autophagy. Chromatin clumping and fragmentation characteristic of typical apoptosis are rarely observed in the degenerating tumor cells; instead, some AV-containing cells exhibit mild pyknosis typical of cells undergoing autophagic degeneration (Fig. 3 C, b and d).

To determine whether AV accumulation occurred in tumor cells before morphological signs of degeneration, we examined U87MG tumors with either 5 d or 3 wk of Akt KD. In tumors expressing shAkt123 for 5 d, most cells showed similar gross morphology to vehicle-treated controls, but with an approximately twofold increase in the percent AV area (from 0.78% in the control tumors to 1.53% in Dox-treated tumors; $P < 0.05$; Fig. 3 C, e–h). After 3 wk of Akt KD, U87MG tumors show signs of degeneration in many cells similar to PC3 tumors treated for 15 d (unpublished data).

Lysosomotropic agents accelerated cell death in PC3 cells with Akt KD

Despite the elevated levels of autophagy and mild cell cycle delay, PC3 cells expressing shAkt123 can survive in culture for many passages under 10% FBS without appreciable increase in cell death. Even under reduced serum (0.5% FBS), there is only marginal decrease in viability over a prolonged period

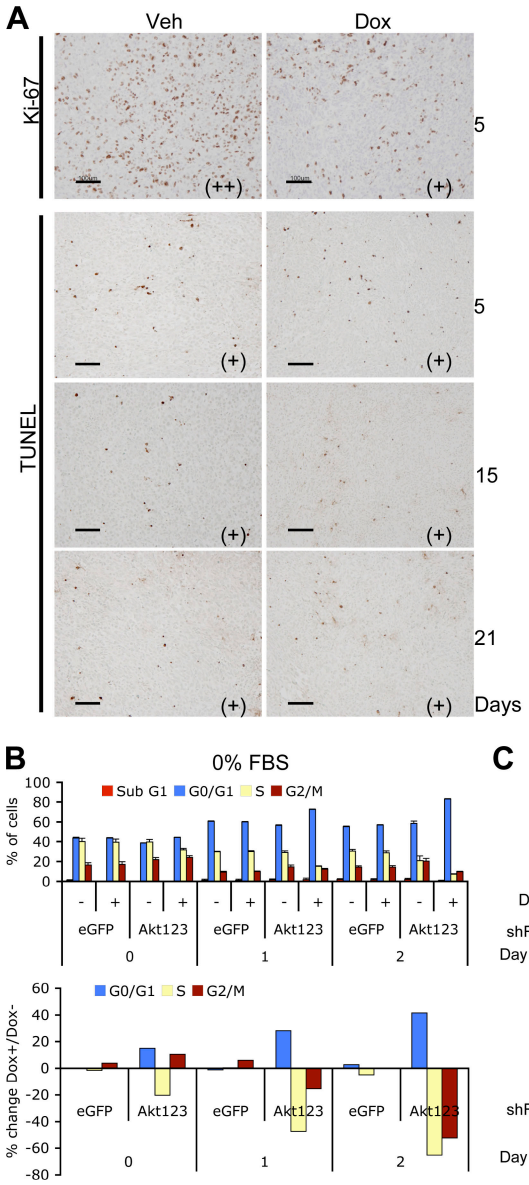

Figure 2. **Akt KD resulted in cell cycle delay without substantial apoptosis.** (A) Histological analysis of PC3-shAkt123 tumors treated with Dox or vehicle control for 5, 15, or 21 d as indicated. Tumor tissues were analyzed by IHC using antibodies specific for Ki-67 or by the TUNEL assay. Pathologist's scoring of the signal intensity for each sample is indicated in parentheses. Bars, 100 µm. (B and C) Effect of triple-Akt KD on cell cycle progression under serum starvation (ss) compared with cells grown under 10% FBS. Cells containing shRNAs targeting EGFP or all three Akts were pretreated for 2 d with or without Dox in medium containing 10% FBS and changed to 0% (B) or 0.5% (C) FBS. Cell cycle profiles were analyzed at the indicated time points after serum withdrawal. Error bars represent SEM (n = 3). The percentage of change in each cell cycle phase with Dox versus without Dox treatment is also shown.

(unpublished data). Although the literature has been controversial on the effect of early stage autophagy inhibition on cell survival, blocking autophagy at a late stage has been more consistently shown to cause accelerated cell death under autophagy-inducing conditions (Kanzawa et al., 2004; Boya et al., 2005; Gonzalez-Polo et al., 2005; Kroemer and Jaattela, 2005; Yu et al., 2006). Therefore, we investigated the effect of blocking the completion of autophagy initiated by Akt KD on cell viability. In PC3-shAkt123 cells stably expressing GFP-LC3, Akt KD resulted in punctate GFP signals (Fig. 4 A and Fig. S2 E) with a corresponding reduction of the nonlipidated precursor form of the endogenous LC3 (LC3-I) and a slight increase in the lipidated autophagosome-localized LC3-II, which is rapidly turned over in the autolysosomes (Fig. 4 B; Klionsky et al., 2008). The lysosomotropic agent chloroquine (CQ), a weak base amine widely used to inhibit the maturation of autophagosomes into degradative autolysosomes (Boya et al., 2005; Kroemer and Jaattela, 2005; Lum et al., 2005), caused the appearance of small GFP-LC3 clusters in the perinuclear region. The combination of CQ with Akt KD resulted in a much stronger accumulation of GFP-LC3 dots as well as augmented accumulation of LC3-II in the presence of continued LC3-I turnover, consistent with a defect in autolysosomal degradation. Similar accumulation of MDC^+ vacuoles was also observed (Fig. S2 F). This was accompanied by an accelerated cell death in shAkt123-expressing cells treated with CQ under 0.5% and, more pronouncedly, 0% FBS (Fig. 4, C and D).

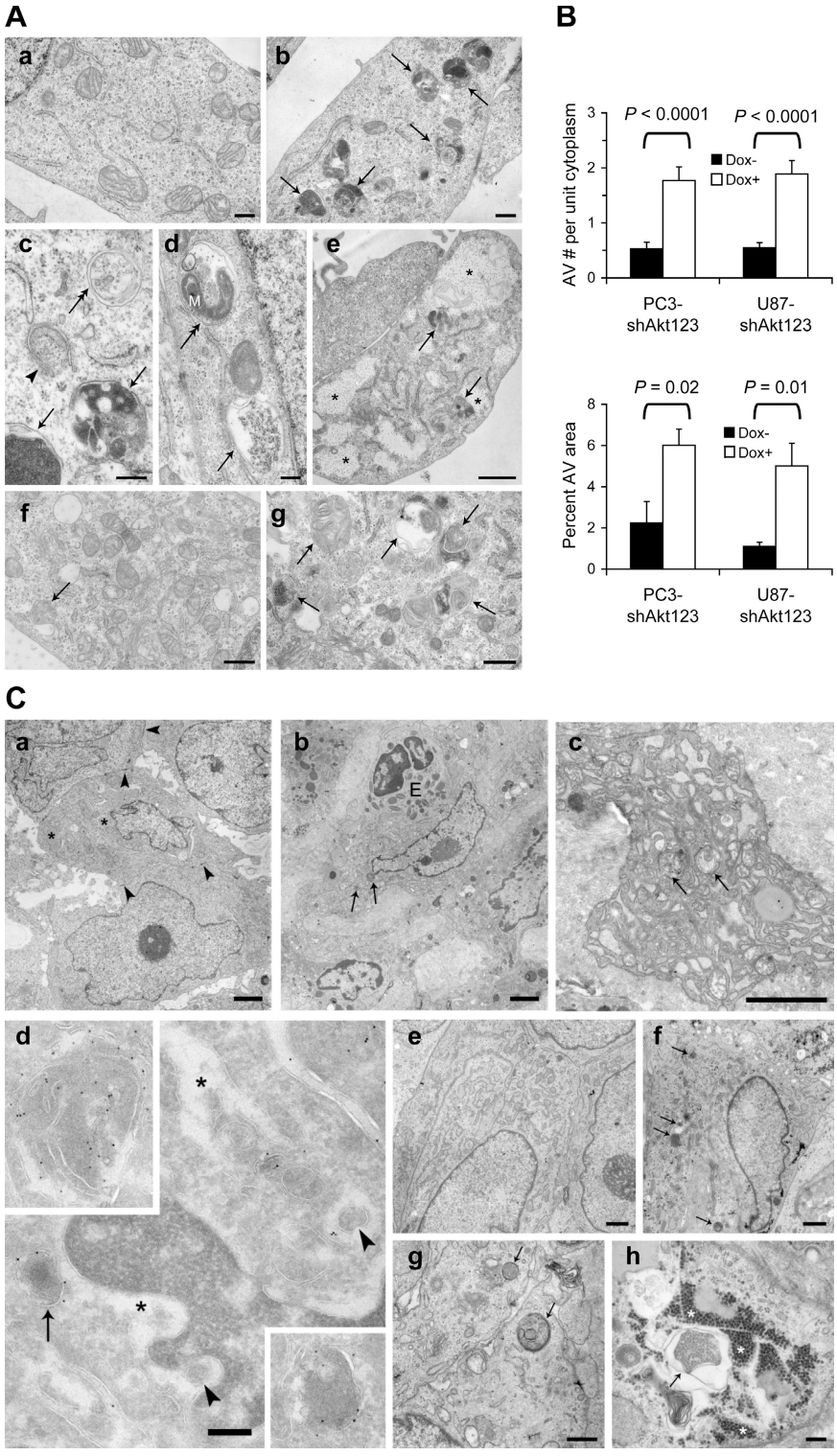

Figure 3. **Autophagy was induced in PC3 and U87MG cells by Akt KD.** (A) EM images of PC3 (a–d) and U87MG (e–g) cells grown in the absence (a and f) or presence (b–e and g) of Dox-induced Akt123 KD for 5 d. Arrows, degradative autolysosomes. Double arrows, initial AVs. Arrowhead, phagophore isolation membrane. M, mitochondrion in an AV. Asterisks, glycogen particle clusters. Bars: (a, b, f, and g) 0.5 µm; (c and d) 200 nm; (e) 1 µm. (B) Quantification of the number of AVs per unit cytoplasmic area of 4.5 μm^2 ($n \geq 64$) and the percentage of cytoplasmic area occupied by AV in randomly sampled cytoplasmic areas ($n = 5$ areas of >200 μm^2) of PC3 and U87MG cells with and without Dox-induced shAkt123 expression. Error bars represent SEM. (C) Dox-induced Akt silencing caused degeneration in PC3 and U87MG tumors. (a) PC3 tumors expressing the control EGFP shRNA after 15 d of Dox treatment. The tumor cells contain large nuclei and nucleoli, some lipid droplets (asterisks), and are connected by cell junctions (arrowheads). (b–d) PC3 tumors expressing shAkt123 after 15 (b and c) or 10 d (d) of Dox treatment. (b) Cells and nuclei in these tumors often appear shrunken. Arrows, AVs. E, eosinophil. (c) Two AVs (arrows) found among dilated RER cisternae in a degenerating tumor cell. (d) Ultrathin cryosection with immunogold labeling of human LAMP1. Label occurs on lysosomes (arrow) and AVs (top inset). Some of the tumor cells also contain human LAMP1–positive dense bodies with a shape reminiscent of microautophagy (bottom inset; de Waal et al., 1986). The tumor cells have widened nuclear envelope and ER cisterns (asterisks), which contain small cytoplasmic islands (arrowheads). (e) U87MG tumor after 5 d of vehicle treatment. (f–h) U87MG-shAkt123 tumor after 5 d of Dox treatment. Arrows, AVs. (h) In some tumor samples, cells with glycogen clusters (asterisks) and glycogen-containing AVs occur. Bars: (a–c) 2 µm; (e and f) 1 µm; (g) 0.5 µm; (d and h) 200 nm.

A second lysosomotropic agent, bafilomycin A1 (Ba), which inhibits the vacuolar proton pump (V-H^+-ATPase) and prevents the proper acidification of lysosomal compartments (Yamamoto et al., 1998), also promoted cell death in combination with shAkt123. Increased annexin V–positive population and caspase-3,7 activity was observed in cells treated with either CQ or Ba in combination with Akt KD, correlating with an increase in poly-ADP-ribose polymerase (PARP) cleavage in these cells (Fig. 4 B). In contrast, pretreatment with 1 mM 3-MA, an inhibitor of the earliest stage of autophagosome formation, attributed to its inhibition of class III PI3K (Seglen and Gordon, 1982; Petiot et al., 2000), suppressed the cell death–promoting effect of either CQ or Ba on shAkt-expressing cells (Fig. 4, C and D). This suggests that the accelerated cell death caused by the lysosomotropic inhibitors is dependent on the accumulation of abnormal AVs.

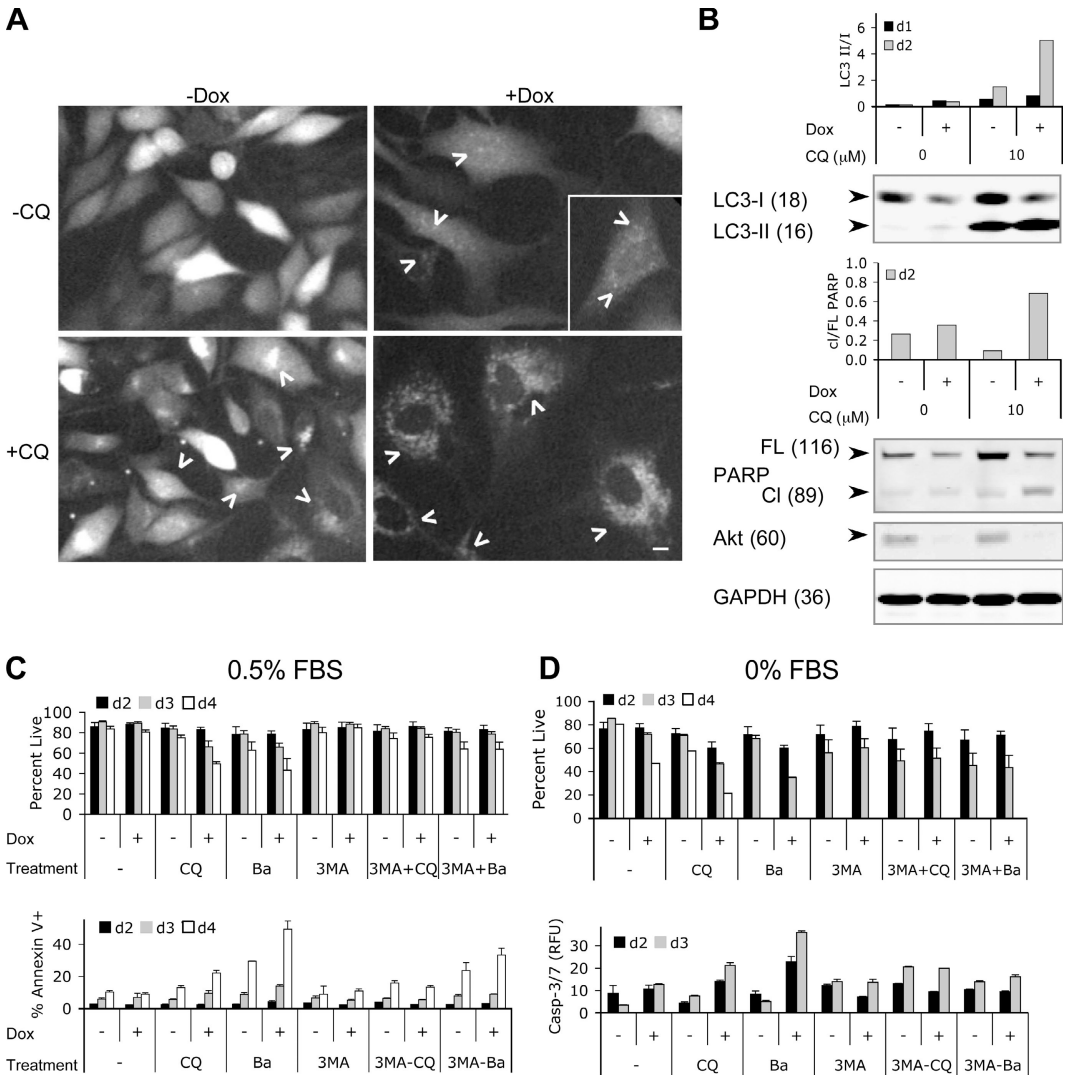

Figure 4. **Lysosomotropic agents accelerated cell death in combination with Akt KD.** (A) CQ treatment caused accumulation of GFP-LC3 dots in Dox-treated PC3-shAkt123 cells. PC3-shAkt123 cells stably expressing GFP-LC3 were pretreated with or without 1 μg/ml Dox for 6 d and treated with or without 10 μM CQ. GFP fluorescence was imaged after 1 d of CQ treatment. Arrowheads point to representative GFP dots or clumps. Bar, 10 μm. (B) Effect of shAkt123 and 10 μM CQ on LC3 processing, PARP cleavage, and total Akt in PC3-shAkt123 cells treated with or without Dox or CQ. The ratios of LC3-II to LC3-I and cleaved (Cl) to full-length (FL) PARP were quantified from immunoblots of cell lysates made at days 1 and 2 of CQ treatment. Immunoblots of day 2 samples are shown. Molecular masses are indicated in kilodaltons parenthetically next to each protein. Data are representative of three independent experiments. (C) CQ promoted cell death in PC3 cells induced to express shAkt123, whereas 3-MA pretreatment delayed this effect. PC3-shAkt123 cells were preincubated with 1 μg/ml Dox and/or 1 mM 3-MA for 3 d before 10 μM CQ or 2.5 nM Ba was added. Cell viability was determined at days 2, 3, and 4 under 0.5% (C) or 0% (D) FBS after CQ or Ba was added. The percentage of the annexin V–positive PI-negative population was determined at days 2, 3, and 4 under 0.5% FBS. Caspase-3/7 activity was determined at days 2 and 3 under 0% FBS and expressed as relative fluorescence units (RFU, in thousands) normalized to the same number of cells. Error bars represent SD of three independent experiments.

CQ accelerated cell death in combination with PI3K and Akt inhibitors

Recently, a phosphatidylinositol ether lipid analogue that inhibits Akt activation was reported to induce autophagy with radiosensitizing effect (Fujiwara et al., 2007). Because phosphatidylinositol ether lipid analogues are known to have additional cellular targets (Gills et al., 2006; Memmott et al., 2008), we asked whether other specific inhibitors of PI3K–Akt could also induce autophagy and sensitize cells to late stage autophagy inhibition. We first used a dual PI3K/mTOR inhibitor, PI-103, which inhibits the class I PI3Ks and mTOR at nanomolar concentrations but is >1,000-fold less potent on the class III PI3K (Knight et al., 2006). In contrast to the broad-spectrum PI3K inhibitors wortmannin or LY294002, which are equipotent at inhibiting both class I and III PI3Ks and inhibit autophagy because of the latter activity (Petiot et al., 2000; Knight et al., 2006), PI-103 is potent at inducing the accumulation of AVs (Fig. 5, B and C). Similar to Akt KD, combination with CQ accelerated the death of cells treated with PI-103 (Fig. 5 A). The markedly increased LC3-II to LC3-I ratio and the appearance of enlarged vacuoles brightly stained by MDC was observed before the detection of overt cell death (Fig. 5, B and C). As observed with Akt KD, pretreatment with 3-MA reduced both LC3-II to -I ratios and the accumulation of MDC^+ vacuoles and slowed down the rate of cell death

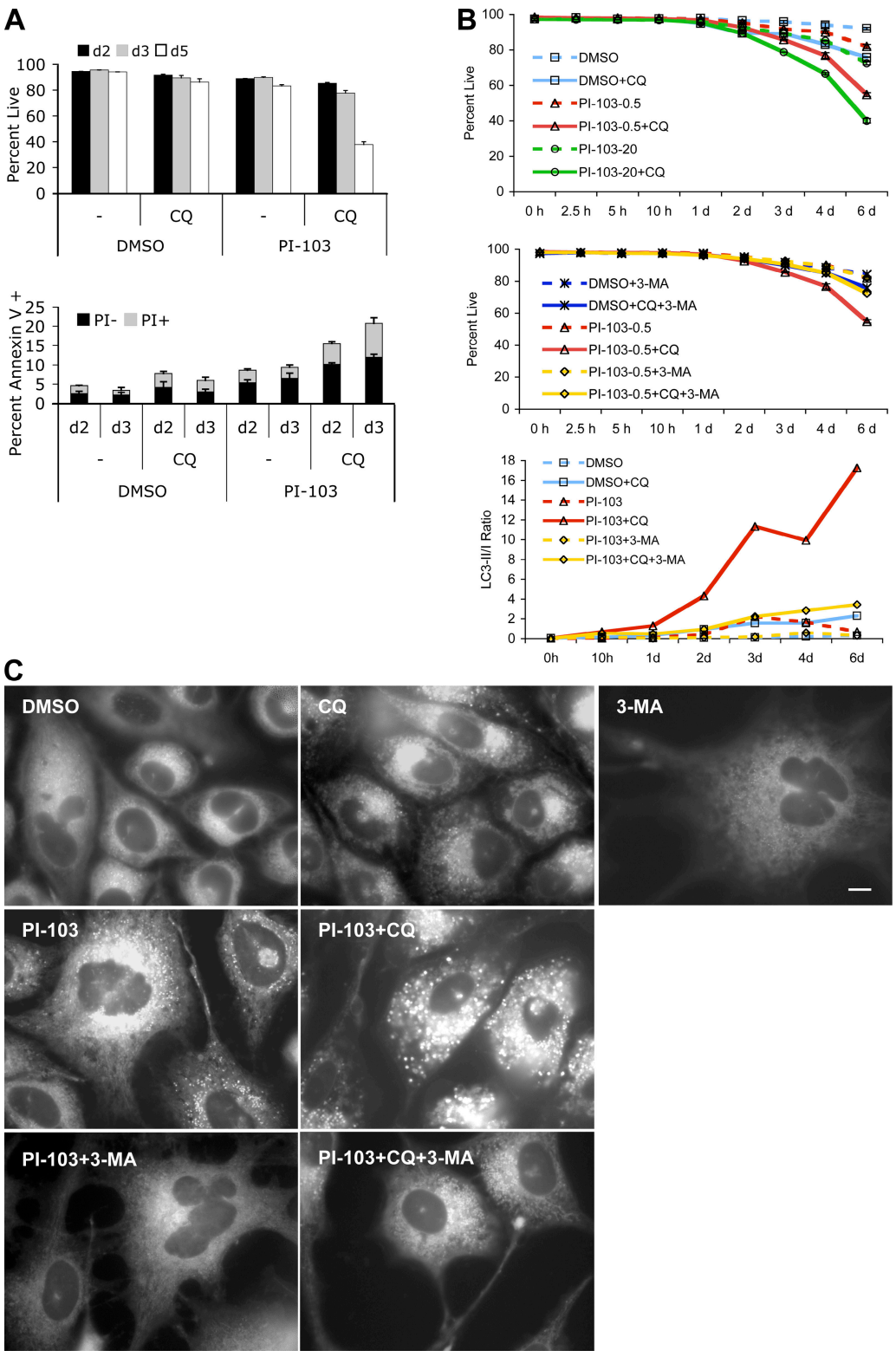

Figure 5. **CQ accelerated cell death in combination with PI-103.** (A) PC3 cells were treated with DMSO or 0.5 μM PI-103 in the presence or absence of 10 μM CQ under 0.5% FBS. Cell viability was determined by PI exclusion at days 2, 3, and 5. Annexin V staining was analyzed at days 2 and 3 and broken down into PI+ or PI− populations. (B) Time course of cell viability in PC3 cells treated with 0.5 (PI-103-0.5) or 20 μM (PI-103-20) PI-103 with or without 10 μM CQ or 3 mM 3-MA. PC3 cells pretreated with PI-103 for 24 h under 1% FBS were split into medium containing 0.5% FBS in the presence or absence of CQ. 3-MA was added immediately before PI-103, 24 h before CQ addition. Cell viability was determined by PI exclusion at the indicated time points after CQ addition. Error bars represent SEM ($n = 3$). LC3-II to LC3-I ratios were determined from quantitation of immunoblots (with 0.5 μM PI = 103. (C) CQ dramatically increased the size and number of MDC^+ vacuoles in PC3 cells treated with PI-103, whereas 3-MA suppressed this effect. Cells were cultured in medium containing 0.5% FBS and treated with DMSO, 0.5 μM PI-103, 10 μM CQ, and 5 mM 3-MA, alone or in combinations as indicated. MDC staining at 48 h is shown. Bar, 10 μm.

(Fig. 5, B and C). In contrast, the cell death–promoting effect of CQ was partially mimicked by siRNA KD of LAMP2, a protein previously shown to be required for the maturation of autophagosomes into autolysosomes (Fig. S3, A and B, available at http://www.jcb.org/cgi/content/full/jcb.200801099/DC1; Gonzalez-Polo et al., 2005).

A similar effect of CQ was also obtained with a selective dual Akt1,2 inhibitor, Akti-1/2 (Barnett et al., 2005). Treatment with Akti-1/2 alone effectively inhibited the phosphorylation of Akt on both Ser473 and Thr308 residues and significantly reduced the phosphorylation of downstream target S6 without causing significant cell death (Fig. 6, A and B). Cotreatment with CQ resulted in a rapid drop in cell viability with complete cell death observed by day 10. Immunoblot analysis revealed a significant accumulation of LC3-II within 24 h of Akti-1/2 treatment, which is further enhanced upon CQ cotreatment (Fig. 6, B and C).

To follow the kinetics of cell death, we used time-lapse microscopy to image live cells treated with CQ and Akti-1/2 (Fig. 7 A and Videos 1–4, available at http://www.jcb.org/cgi/content/full/jcb.200801099/DC1). CQ treatment alone caused a mild decrease in cell division and a gradual accumulation of dark particles in the perinuclear region. AO staining indicates that these particles are AVOs whose formation is inhibited by 3-MA (unpublished data). Treatment with Akti-1/2 alone resulted in near-complete inhibition of cell division without overt cell death. These cells exhibited a flattened morphology with accumulation of AVOs that eventually filled the cytoplasm. Cells treated with both Akti-1/2 and CQ showed similar accumulation of AVOs, but cell shrinkage and plasma membrane rupture was observed within 48 h. On a few occasions, two neighboring cells were found to form a membrane junction that expanded into complete fusion between the two cells before rupture of the plasma membrane (Fig. 7 A, white arrowheads; and Video 4).

Similar correlation between AVO accumulation and cell death was observed using multispectral imaging flow cytometry (Fig. 7, B and C). Treatment with either CQ or Akti-1/2 alone induced AVO accumulation without significant loss of viability, whereas the combination of both resulted in a further increase in AVO accumulation in live cells and a concomitant increase in cells with condensed apoptotic nuclei and the appearance of anucleated population characteristic of necrotic cells.

Autophagy inhibition and degradation-defective autolysosome accumulation both contribute to accelerated cell death induced by CQ in combination with Akti-1/2

To investigate whether autophagy inhibition by itself is sufficient to induce accelerated cell death in combination with Akt inhibition, we used siRNA to KD Atg7, a gene involved in the formation of autophagosomes (Ohsumi, 2001). KD of Atg7 alone did not show a significant effect on cell death but induced a small drop in cell viability by day 3 when combined with Akti-1/2. However, when combined with both CQ and Akti-1/2, Atg7 KD resulted in a transient delay of cell death at day 2 (Fig. S3, C and D). Together with the aforementioned effect of 3-MA, these data suggest that autophagy inhibition and defective AV

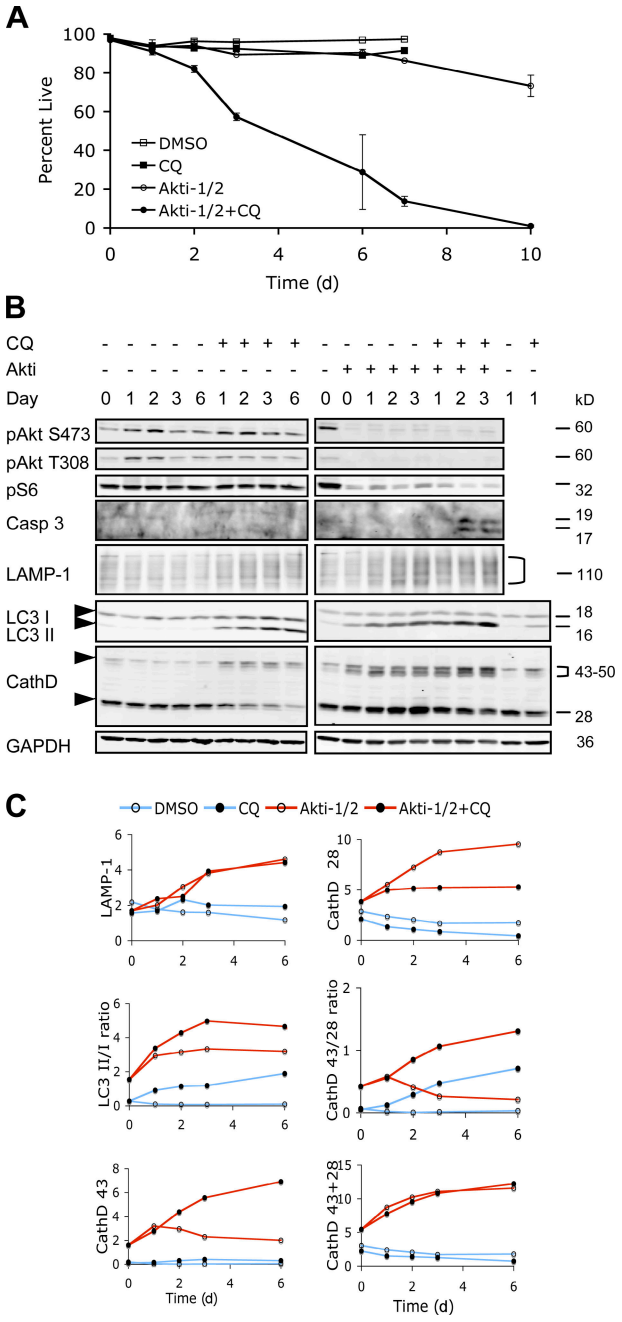

Figure 6. **CQ accelerated cell death in combination with Akti-1/2.** (A) PC3 cells were treated with DMSO or 4 µM Akti-1/2 in the presence or absence of 10 µM CQ under 0.5% FBS. Cell viability was determined by PI exclusion over the course of 10 d. Error bars represent SEM. Representative data from one of three independent experiments are shown. (B) Immunoblot analysis of cell lysates collected at the indicated time points from the experiment shown in A. Arrowheads indicate the positions for LC3-I and -II, CathD 43, and CathD 28. Quantifications of the indicated markers are shown in C. CathD 43, the 43–50-kD forms of cathepsin D precursors. CathD 28, the 28-kD cathepsin D heavy chain.

accumulation both contribute to the accelerated cell death induced by CQ in combination with Akt inhibition.

Because autophagy is a key function of the lysosomal compartment (Terman et al., 2006), we examined the lysosomal marker LAMP1 and cathepsin D, the predominant lysosomal aspartic protease, by immunoblotting (Fig. 6, B and C). Akti-1/2

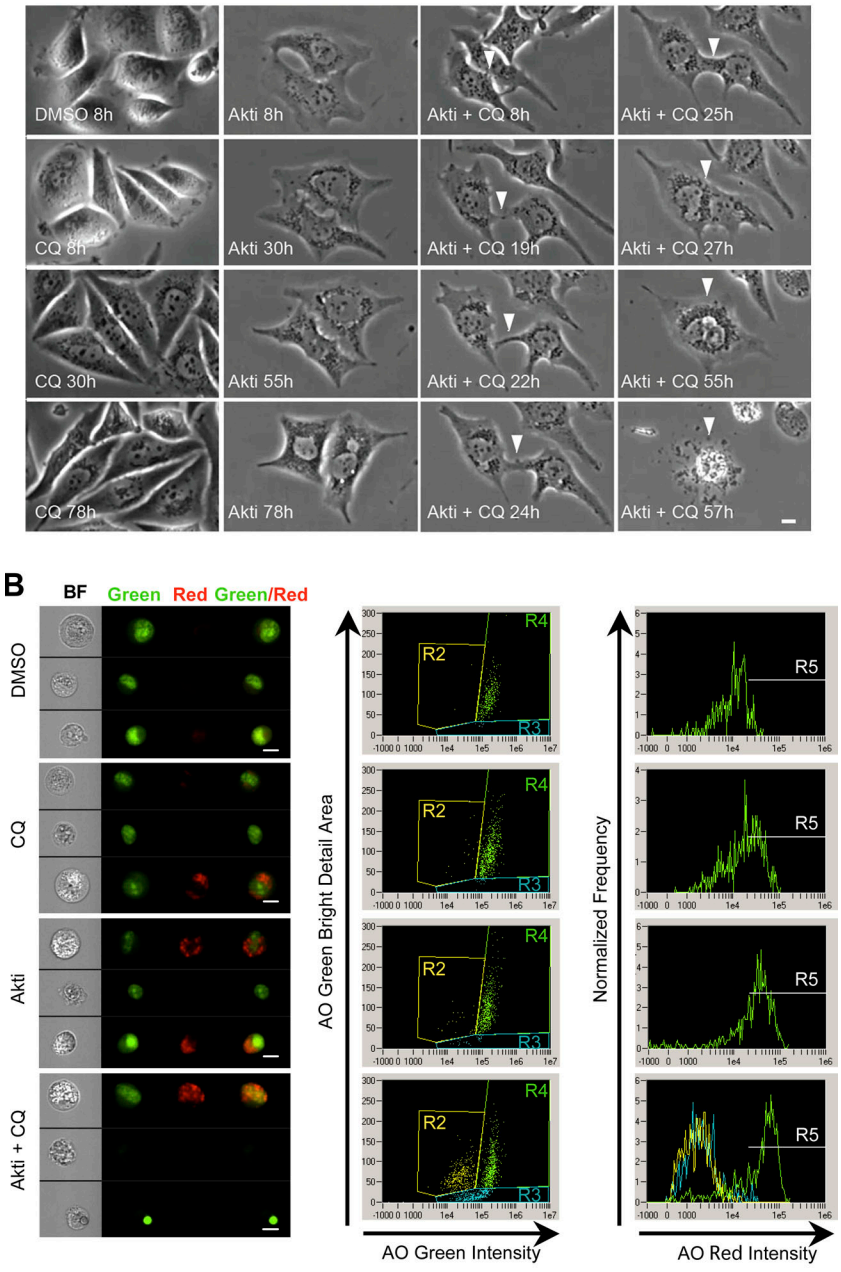

Figure 7. **Accumulation of AVOs preceded plasma membrane rupture and correlated with the appearance of apoptotic and anucleated cells with Akti-1/2 and CQ treatment.** (A) PC3 cells treated with DMSO, 10 µM Akti-1/2, 10 µM CQ, or both under 5% FBS were followed for 3 d using time-lapse microscopy. Representative images of the cells at the indicated time points are shown. White arrowheads indicate the fusion between two adjacent cells before plasma membrane rupture in cells treated with both agents. Full time-lapse videos are available in Videos 1–4, available at http://www.jcb.org/cgi/content/full/jcb.200801099/DC1. Bar, 10 µm. (B) PC3 cells treated with the indicated agents were stained with AO and analyzed by multispectral imaging flow cytometry. (left) Brightfield (BF), nuclei (green), vacuoles (red), and green/red composite images of three representative cells with each treatment are shown. Bars, 10 µm. (middle) plotting AO green intensity versus AO green bright detail area revealed three distinct populations: R2 anucleated cells, R3 apoptotic cells, and R4 live cells. (right) AO red intensity for R4 is plotted on the histogram with an arbitrary gate (R5) drawn to include events with the brightest AO red intensity. R2, R3, and R4 histograms are overlaid in the Akti + CQ plot only. (C) Statistics for each population shown in B. *, percentage of total single cells; **, mean fluorescence intensity of R4 live cells; ***, percentage of R4 live cells.

C

Sample	CQ	Akti-1/2	Anucleate (R2) %*	Apoptotic (R3) %*	Live (R4) %*	AO Red MFI**	AO Red (R5) %***
1	-	-	0.6	2.5	96.5	10739	7.2
2	+	-	2.4	2.8	94.2	19414	44.6
3	-	+	5.0	5.9	88.6	32018	67.1
4	+	+	26.8	27.4	44.9	48989	72.2

alone induced an increase in LAMP1 levels, consistent with an elevated lysosomal activity. Cathepsin D is synthesized as a 43-kD preprocathepsin D that is cleaved cotranslationally and glycosylated to form a 46-kD procathepsin D, which is targeted to lysosomes yielding an intermediate that is further cleaved into a mature enzyme consisting of a 15- kD light chain and a 28-kD heavy chain. Using an antibody that detects both the 28-kD and the precursor forms of cathepsin D, an increase in the level of the premature forms of cathepsin D at 43–50 kD was first detected after Akti treatment alone followed by an increase in the 28-kD heavy chain of the mature enzyme, again indicating an increased lysosomal activity. CQ caused accumulation of the precursor forms at the expense of the 28-kD chain, consistent with an inhibition of lysosomal cysteine protease activity required for the processing and maturation of cathepsin D (Liaudet-Coopman et al., 2006). In cells treated with both Akti and CQ, the precursor forms of cathepsin D accumulated to even higher levels than either alone, whereas the mature 28-kD chain decreased gradually.

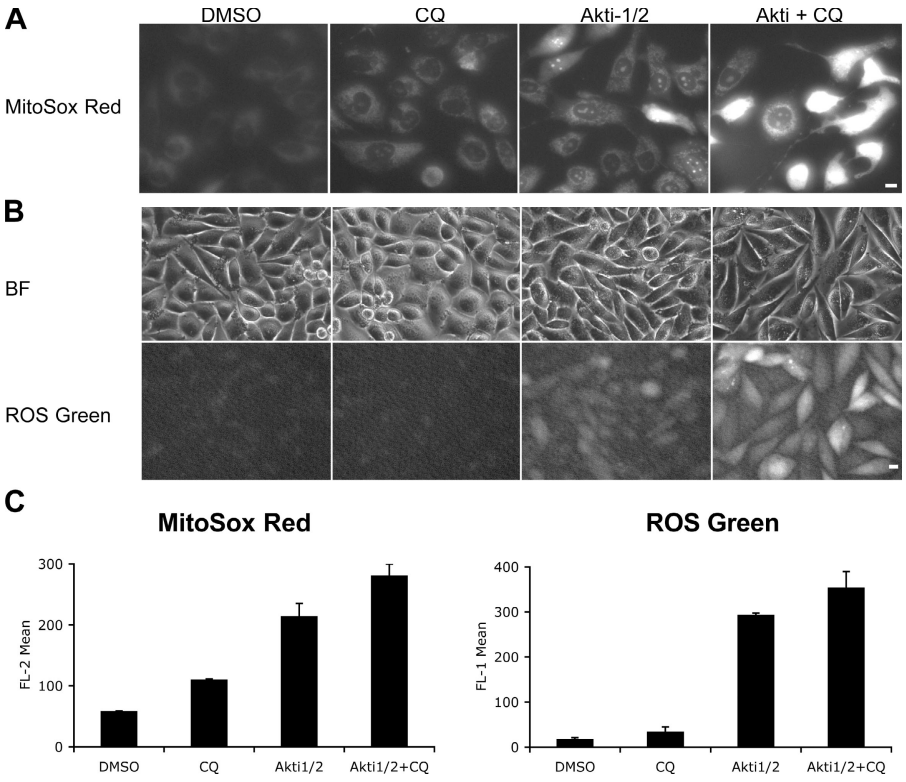

Figure 8. **Akt inhibition induces mitochondrial superoxide and cellular ROS production, which is augmented by CQ.** (A) PC3 cells cultured in 0.5% FBS were treated with DMSO, 3 μM Akti-1/2, 10 μM CQ, or both, stained with MitoSOX red dye, and examined by fluorescence microscopy. Images at 24 h are shown. Bar, 10 μm. (B) PC3 cells treated as in A were stained with the Image-iT LIVE green ROS Detection kit and examined by fluorescence microscopy at 24 h. Bright field (BF) images of cells are also shown. Bar, 10 μm. (C) Quantification of MitoSOX red and ROS green fluorescence intensities by flow cytometry at 24 h. Cells were treated as in A and B. Error bars represent SEM (n = 3).

Akti treatment also reduced the level of p62, another marker of autophagic activity that is degraded in the autolysosomes (Klionsky et al., 2008), whereas CQ blocked p62 degradation both with and without Akti treatment (Fig. S5 C, available at http://www.jcb.org/cgi/content/full/jcb.200801099/DC1).Collectively, these data suggest that Akt inhibition causes an increased production and maturation of the lysosomal enzymes, whereas CQ cotreatment impairs the maturation of these enzymes in the final autolysosomal compartment, causing accumulation of defective AVOs. The latter is accompanied by an increased cleavage of caspase 3 into the active forms within 2 d (Fig. 6 B) with a corresponding increase in caspase activity and cleavage of its substrate PARP (unpublished data). zVAD.fmk, a pancaspase inhibitor, partially rescued cell death at all concentrations tested (Fig. S3 E). Although zVAD.fmk can also inhibit lysosomal cysteine proteases at higher concentrations, and the latter have been reported to mediate caspase-independent cell death (Foghsgaard et al., 2001), neither of the broad-spectrum cysteine protease inhibitors zFA.fmk and ALLN (*N*-Acetyl-Leu-Leu-Nle-CHO) nor a more specific cathepsin B inhibitor CA-074-Me showed significant rescue of cell death induced by Akti and CQ. Instead, the cysteine protease inhibitors enhanced cell killing in combination with Akti at 10–50 μM-concentrations, although they also showed cytotoxicity alone at higher concentrations (Fig. S3, F–H). These results suggest that cell death induced by Akti and CQ is at least partially caspase dependent, whereas lysosomal protease activity may be required for the survival of cells under Akt inhibition.

To further ask whether impaired lysosomal degradation can accelerate cell death in combination with Akt inhibition, we knocked down cathepsin D using siRNA. Indeed, this significantly increased cell death when combined with Akti-1/2 and further enhanced the cell-killing effect of CQ when both are combined with Akti (Fig. S3 I). Similarly, pepstatin A, an inhibitor of aspartic proteases including cathepsin D, also promoted cell death together with Akti-1/2 (Fig. S3 J).

CQ augmented Akti-induced mitochondrial superoxide and cellular reactive oxygen species (ROS) accumulation

Increasing evidence has suggested an intimate relationship between lysosomes and mitochondria in the execution of programmed cell death (Bursch, 2001; Terman et al., 2006). Therefore, we examined the effect of Akt inhibition and CQ on mitochondrial membrane potential. Consistent with Akt's function in maintaining mitochondrial integrity (Parcellier et al., 2008), Akti-1/2 alone caused a decrease in mitochondrial membrane potential, although significant numbers of polarized mitochondria were still present in the majority of cells. Although CQ alone did not have a significant effect, cotreatment of CQ and Akti-1/2 caused an almost complete loss of mitochondrial potential, preceding the sharp drop in cell viability (Fig. S4, A and B, available at http://www.jcb.org/cgi/content/full/jcb.200801099/DC1).

It has recently been reported that mitochondrial ROS is involved in autophagy induction (Scherz-Shouval et al., 2007). Because mitochondria are the primary intracellular source of superoxide ($O_2^{\cdot -}$) generation, we analyzed $O_2^{\cdot -}$ production using MitoSOX red, an $O_2^{\cdot -}$ indicator that accumulates in the mitochondria as a function of membrane potential and fluoresces upon oxidation and subsequent binding to DNA. Akti-1/2 alone increased MitoSOX fluorescence within 6 h (Fig. 8, A and C; and not depicted). Most of the fluorescence exhibited a mitochondrial localization pattern with a subpopulation of cells showing

nuclear fluorescence, consistent with increased mitochondrial permeability in these cells. Although CQ alone only caused a mild increase in MitoSOX signal, the combination with Akti-1/2 resulted in a significant increase in fluorescence intensity with most cells exhibiting a strong nuclear staining pattern. The increase in $O_2^{\cdot -}$ production was followed by an increase in overall cellular ROS levels within 24 h, as measured using a general ROS-sensitive probe (Fig. 8, B and C). Interestingly, cytoplasmic ROS signal induced by Akti-1/2 alone was attenuated within 48 h, whereas cotreatment with CQ caused a prolonged increase in ROS levels (Fig. S4 D and not depicted). This is consistent with the notion that limited mitochondrial depolarization caused by Akt inhibition induces a transient ROS signal to increase autophagy, which in turn removes the damaged mitochondria. Impaired digestion of cellular components caused by CQ results in autolysosomal aggregation of deleterious oxidative products such as ceroid/lipofuscin, which can further amplify the ROS damage (Moore et al., 2006), leading to cell death. 3-MA pretreatment reduced ROS levels induced by Akti (Fig. S4 C), suggesting a class III PI3K dependence similar to starvation-induced ROS production (Scherz-Shouval et al., 2007). Treatment with a general ROS scavenger *N*-acetylcysteine (NAC) rescued cell viability in the presence of Akti and CQ (Fig. S5, A and B). In addition, NAC reduced Akti-induced LC3 and GFP-LC3 lipidation, p62 degradation, and GFP-LC3 puncta formation (Fig. S5, C and D), consistent with an essential role of ROS in autophagy induction (Scherz-Shouval et al., 2007).

CQ selectively accelerated cell death in Akti-treated PTEN-null cells in vitro and enhanced the antitumor efficacy of Akt KD in vivo

Because PC3 cells are PTEN null, we explored whether PTEN status might affect the sensitivity of cells to Akt inhibition alone or in combination with CQ using isogenic $PTEN^{+/+}$ and $PTEN^{-/-}$ mouse embryonic fibroblasts (MEFs). The $PTEN^{-/-}$ MEFs were previously shown to have elevated Akt pathway activity and are more sensitive to the antiproliferative effect of mTOR inhibition than $PTEN^{+/+}$ MEFs (Sun et al., 1999). As shown in Fig. 9 A, the $PTEN^{-/-}$ MEFs were also significantly more sensitive to the cell-killing effect of combined CQ and Akti-1/2 than their $PTEN^{+/+}$ counterparts. This suggests that $PTEN^{-/-}$ cells may be more dependent on autophagic degradation for survival upon Akt inhibition, raising the possibility that a reasonable therapeutic index may be achievable by selective targeting of the malignant PTEN-null tumor cells using this strategy.

To ask whether PTEN-null tumors also rely on autophagic degradation upon Akt inhibition in vivo, we examined the effect of CQ on the survival of PC3 xenograft tumors expressing shAkt123. As shown in Fig. 9 B, intraperitoneal injection of CQ alone caused a small but insignificant reduction in tumor growth rate. Akt KD alone resulted in significant tumor growth inhibition with an initial tumor stasis, but most tumors failed to regress completely, and rebound occurred in 90% of the tumors within 2–3 wk; no complete remission was achieved. In contrast, complete regression was observed in 40% of the tumors treated with both Dox and CQ with stasis maintained in another 20% of the tumors throughout the study (Fig. 9, C and D). Similar results were obtained with a subcutaneous peritumor injection of CQ (unpublished data). EM examination of tumor samples taken at day 5 revealed a mild increase in the AV area in tumors treated with either Dox or CQ alone, whereas a dramatic accumulation of AVs was observed in a tumor treated with both Dox and CQ that showed >50% regression. These AVs are larger than those found in the Dox- or CQ-alone tumors and contain dense undigested materials, but usually with a single-membrane autolysosomal appearance and stained positive for human LAMP1, consistent with impaired degradation after autophagosome–lysosome fusions. This coincides with an increased number of tumor nuclei exhibiting apoptotic morphology as well as AV-containing cell debris with compromised plasma membrane integrity and abnormal mitochondria (Fig. 10 and not depicted). Thus, CQ not only accelerated cell death in combination with Akt inhibition in vitro but also increased the incidence of complete tumor remissions in vivo.

Discussion

Using a Dox-inducible shRNA approach, we specifically knocked down each Akt isoform, both individually and in all possible combinations, to evaluate their requirement in the maintenance of tumor growth. Our results suggest that in the PTEN-null PC3 and U87MG cells, Akt1 is the most important isoform, whereas Akt2 and Akt3 activities could partially compensate for the reduced Akt1 activity in maintaining tumor growth. Taking together both the potential metabolic side effects of Akt2 inhibition and the reported increase in invasiveness associated with inhibiting Akt1 alone that could be counteracted by simultaneous inhibition of Akt2 (Irie et al., 2005), it may be necessary to inhibit two or all three Akt isoforms simultaneously to achieve maximum tumor inhibition, but with different degrees of inactivation to preserve crucial levels of isoform activities to reduce side effects.

One of the most prominent functions of Akt is cell survival. Constitutively active Akt has been reported to protect cells from programmed cell death after various proapoptotic insults (Downward, 1998). However, whether apoptosis is a primary response to Akt inhibition is less clear, especially in cancer cells where apoptosis is often suppressed because of various genetic alterations. Previous experiments using small molecule inhibitors of the PI3K–Akt pathway often generate conflicting results that are obscured by their nonspecific effects. Our data indicate that specific KD of Akt can cause cell cycle delay without promoting significant apoptosis. This is consistent with a recent study that only a small portion of total Akt activity is required for apoptosis inhibition (Liu et al., 2006). In contrast, we found that autophagy is a more sensitive response to reduced Akt activity caused by either specific shRNA KD or selective inhibitors of the pathway.

Several mechanisms may contribute to autophagy induction by Akt inhibition. First, inhibiting Akt can lead to mTORC1 inhibition. mTOR is a known inhibitor of autophagy. Interestingly, a constitutively active form of Akt suppressed the induction of autophagy by rapamycin (Takeuchi et al., 2005), raising

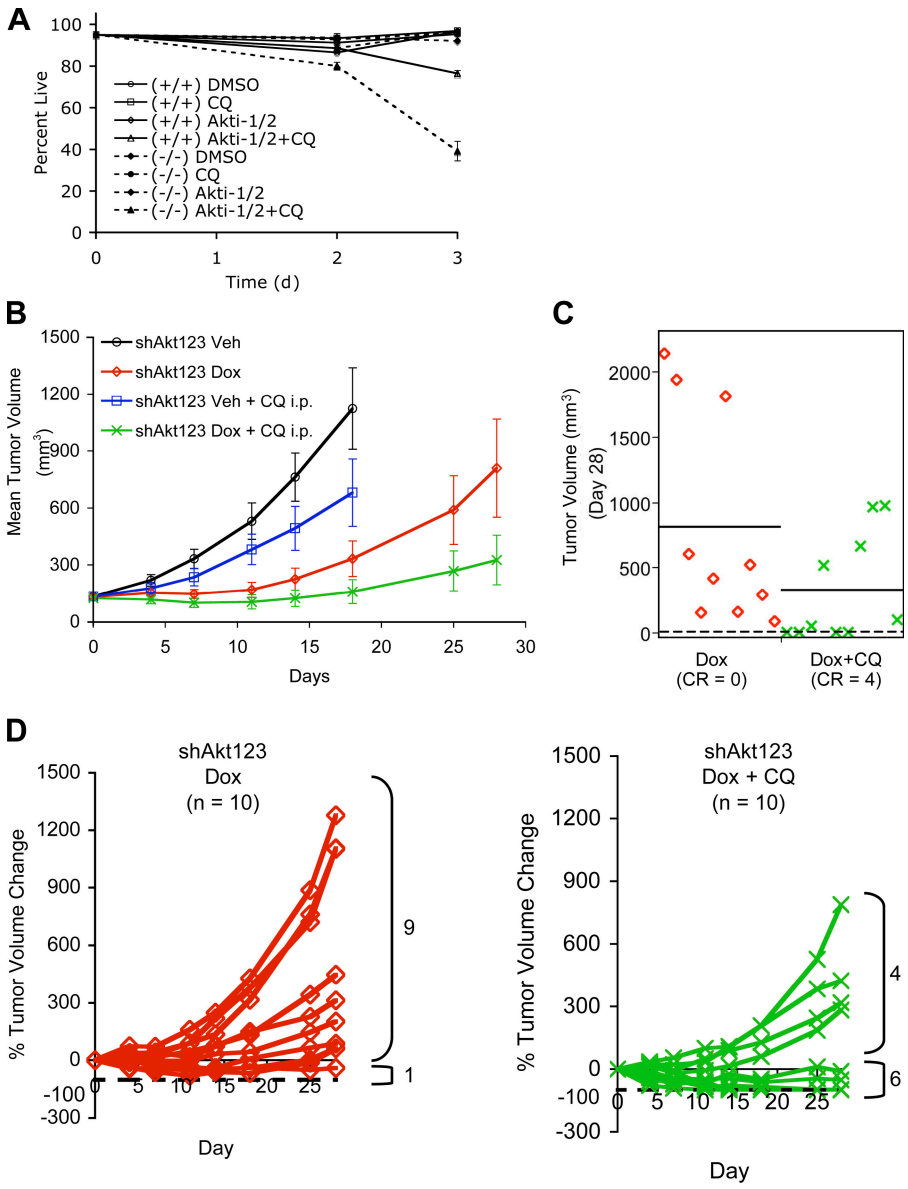

Figure 9. **CQ selectively accelerated cell death in Akti-treated PTEN-null cells in vitro and enhanced the antitumor efficacy of Akt KD in vivo.** (A) PTEN$^{-/-}$ (−/−) MEFs were more sensitive than isogenic PTEN$^{+/+}$ (+/+) counterparts to the combined treatment with Akti-1/2 and CQ. MEFs were treated with 5 µM each of Akti-1/2 and CQ under 1% FBS, and cell viability was determined at days 0, 2, and 3 by PI exclusion. Error bars represent SEM (n = 3). (B) Mean tumor volumes of PC3 xenograft tumors treated daily with vehicle (Veh), Dox only, CQ only, or both Dox and CQ over a 28-d period. The vehicle and vehicle + CQ groups were followed for up to 18 d before terminated because of weight loss from the tumor burdens. Error bars represent SEM (n = 10 tumors in each cohort). (C) Scatterplot of the tumor volumes in the Dox only and Dox + CQ groups on day 28 (P = 0.05). Horizontal bars indicate mean tumor volumes. Numbers of tumors with complete remission (CR, dashed line) are indicated for each group. (D) Individual tumor growth plotted as a percentage of tumor volume change compared with day 0 for the Dox only and Dox + CQ cohorts shown in B. Dashed lines indicate −100% change from the starting tumor volumes, i.e., complete tumor regression. Numbers of tumors with smaller (<0% change) or larger (>0% change) than the starting tumor volumes on day 28 are indicated.

the possibility that the effect of rapamycin on autophagy may be mediated at least partially through inhibiting Akt via its long-term effect on mTORC2 (Sarbassov et al., 2006). Second, other signaling outputs of Akt, such as the FoxO proteins (Zhao et al., 2008) or glucose metabolism, can also contribute to autophagy regulation independently of mTOR. Third, our data indicate that Akt inhibition induces increased mitochondrial superoxide and cellular ROS signals that can activate autophagy.

Autophagy activation may lead to eventual cell death when allowed to reach its limit or may sensitize cells to additional death-inducing stimuli either through eventual autophagic cell death or switching to a more rapid death program such as apoptosis. For example, Akt inhibition may increase radiosensitivity through augmenting autophagic response (Fujiwara et al., 2007), whereas calpain-mediated cleavage of Atg5 may switch autophagy into apotosis (Yousefi et al., 2006). Here we show that inhibiting Akt alone is ineffective in cell killing in the PTEN-null cancer cells that we examined, but cell death can be accelerated through blocking autolysosomal degradation. Although autophagy may be a potential mechanism by which Akt inhibition restricts tumor growth, it may also provide temporary relief from the metabolic and oxidative stress imposed by Akt inhibition. Inhibiting autophagy at an early stage may prevent this temporary protective effect but may also counteract its tumor inhibitory effect while allowing early escape via alternative survival mechanisms. Blocking lysosomal function after tumor cells have become committed and reliant on autophagic degradation, however, might avoid this counteracting effect while amplifying the oxidative damage and cytotoxic effects through accumulation of deleterious oxidative aggregates (Seehafer and Pearce, 2006). Indeed, our data suggest that a compatible lysosomal degradation capacity is critical for cell survival in the presence of elevated autophagic activity induced by Akt inhibition such that inhibiting lysosomal function with lysosomotropic agents, cathepsin D KD or lysosomal protease inhibitors, can all precipitate cell death in combination with Akt inhibition.

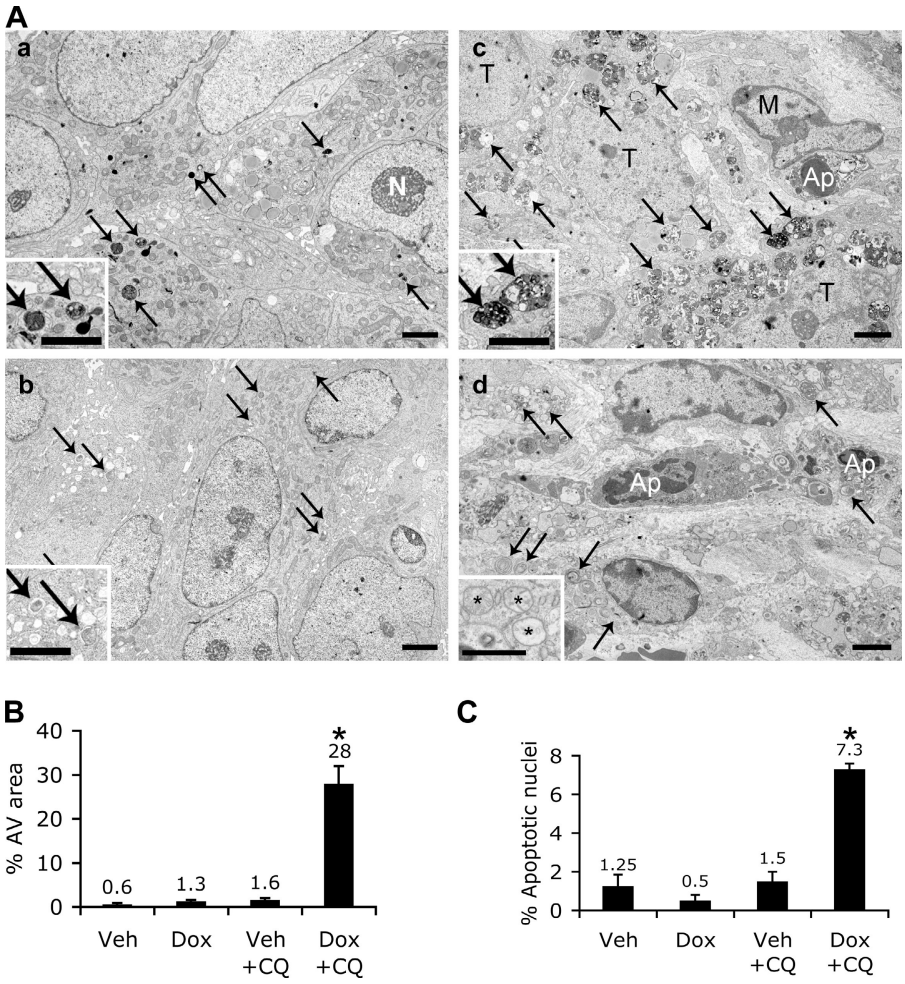

Figure 10. **Increased AV accumulation and apoptosis in PC3 tumor with combined Akt123 KD and CQ treatment.** (A, a) EM images of PC3-shAkt123 tumors treated for 5 d with CQ only. Arrows, dense AVs and lysosomes; N, nucleolus. (b) Dox only. Arrows, AVs with a less dense appearance than in a. (c and d) Both Dox and CQ. (c) Numerous dense and enlarged AVs (arrows) accumulate in tumor cells. An apoptotic cell (Ap) is partially surrounded by a macrophage (M). T, tumor cell. (d) Apoptotic nuclei (Ap) among the AV-loaded (arrows) tumor cells. Insets, enlarged images of AVs (a–c) and abnormal mitochondria (*) in each tumor. Bars: (a–c) 2 µm; (d) 1 µm. (B) Quantification of the percentage of cytoplasmic area occupied by AVs in randomly sampled cytoplasmic areas (n = 6 areas of >80 µm^2). (C) Percentage of apoptotic nuclei among randomly sampled tumor cell nuclei (n = 3–4 sets of 100 tumor cell nuclei). (B and C) Error bars represent SEM; *, $P < 0.0005$ compared with the other three groups.

Autophagy, lysosomal changes, and oxidative stress have been associated with a lengthening list of anticancer treatments, and lysosomotropic agents have shown anticancer activity either alone or in combination with other therapeutic agents (Shoemaker and Dagher, 1979; Ohta et al., 1998; Ostenfeld et al., 2005; Amaravadi et al., 2007; Carew et al., 2007; Fujiwara et al., 2007; Groth-Pedersen et al., 2007). Here we report that autophagy induced by Akt/PI3K/mTOR inhibition can also be exploited using lysosomotropic agents, such as the well-tolerated drug CQ, to promote the remission of PTEN-null human tumor xenografts. Because this effect is expected to correlate positively with the degree of autophagy induced by a given treatment, creative combination of these agents with potent autophagy inducers, such as inhibitors of the Akt pathway, may profoundly affect their anticancer efficacy.

Materials and methods

Cell culture and reagents

The PTEN$^{-/-}$ and PTEN$^{+/+}$ MEFs were maintained as previously described (Sun et al., 1999). The PC3 and U87MG cells were maintained at 37°C and 5% CO_2 in DME/Ham's F-12 (1:1) containing 10% tetracycline-free FBS (Invitrogen). Akti-1/2 was obtained from EMD (Akt inhibitor VIII; Barnett et al., 2005). To inhibit autophagy, cells were treated with 5–10 µM CQ, 2.5 nM Ba, or 1–5 mM 3-MA (all from Sigma-Aldrich) and analyzed at the indicated time points. MitoSOX red mitochondrial superoxide indicator and Image-iT LIVE Green ROS Detection kits were purchased from Invitrogen. The MitoPT Mitochondrial Permeability Transition Detection kit was purchased from Immunochemistry Technologies, LLC.

Inducible shRNA constructs and generation of inducible-shRNA clones

The pHUSH tetracycline-inducible retrovirus gene transfer vector has been described previously (Gray et al., 2005,2007; Hoeflich et al., 2006). The complementary double-stranded shRNA oligos were inserted into this vector system using a shuttle vector followed by a Gateway recombination reaction (Invitrogen) as previously described (Grunwald et al., 2002). The shRNA sequences used in this study are summarized in Table S1. All constructs were verified by sequencing. Retrovirus infection was performed as described previously (Gray et al., 2005; Hoeflich et al., 2006). For single Akt isoform KDs, cells were infected with one retroviral vector encoding an shRNA construct singly targeting each Akt isoform (constructs 252 or 253 for Akt1, 254 or 255 for Akt2, and 259 or 260 for Akt3), and stable clones were selected using 5 µg/ml puromycin. For dual Akt1 and Akt2 KD, a single shRNA targeting both Akt1 and 2 simultaneously (constructs 256 and 257) was used. Dual Akt2 and 3 (constructs 255 and 261) or triple Akt1, 2, and 3 (constructs 257 and 261) KDs were achieved by coinfecting the cells with two retroviral vectors containing different antibiotic selection markers (puromycin and hygromycin), each encoding one single shRNA, and stable clones were selected using 5 µg/ml puromycin and 300 µg/ml hygromycin. For dual Akt1 and 3 KD, either a single shRNA targeting both Akt1 and 3 (construct 258) or coinfection with two shRNA vectors (constructs 253 and 261) was used.

GFP-LC3 stable transfection

DNA construct containing human LC3B tagged at the N terminus with EGFP was transfected into PC3-shAkt123 and PC3 wild-type cells. Stable clones were selected using G418.

Immunoblot analysis, immunohistochemistry (IHC), and TUNEL assay

For immunoblot analysis, total protein lysates were subjected to SDS-PAGE and transferred to nitrocellulose. Antibodies used were anti-Akt1, anti–total-Akt,

anti–p-Akt (Ser473), anti–p-Akt (Thr308), anti–p-S6 (Ser235/236), anti-PARP, and anticleaved caspase-3 (Cell Signaling Technology); anti-Akt2, anti-Akt3, and anti-IRS1 (Millipore); anti–p-PRAS40 and anti-GFP (Invitrogen); anti-$p27^{Kip1}$ (Santa Cruz Biotechnology, Inc.); anti-LC3 (Novus); anti-LAMP2 and anti–cathepsin D (BD Biosciences); anti-p62/SQSTM1 (BIOMOL International, L.P.); anti–β-actin (Sigma-Aldrich); and anti-glyceraldehyde-3-phosphate dehydrogenase (Advanced Immunochemical Inc.). Primary antibodies were detected using IR Dye 800–conjugated (Rockland) and Alexa Fluor 680–conjugated (Invitrogen) species-selective secondary antibodies. Detection and quantification were performed using an infrared scanner (Odyssey; LICOR) using the manufacturer's software. For IHC, formalin-fixed, paraffin-embedded specimens were collected. 5-µm-thick paraffin-embedded sections were stained using an anti–Ki-67 (MIB-1; Dako) antibody with the Animal Research Kit (Dako). Tissues were counterstained with hematoxylin, dehydrated, and mounted. In all cases, antigen retrieval was performed with the Target Retrieval kit (Dako) according to the manufacturer's instructions. For TUNEL assay, formalin-fixed, paraffin-embedded sections were stained using an in situ cell death detection kit (POD; Roche) according to the manufacturer's instructions.

Xenograft study

6–8-wk-old female athymic nude *nu/nu* mice were purchased from Charles River Laboratories and maintained in Genentech's conventional animal facility. Mice were injected in the right flank with 5–7.5 × 10^6 cells resuspended in 200 µl Hank's balanced salt solution (Invitrogen). When tumors reached a mean volume of 100–300 mm^3, the mice with similarly sized tumors were grouped into treatment cohorts. Mice received 5% sucrose or 5% sucrose plus 1 mg/ml Dox in drinking water for control and KD cohorts, respectively. Amber-colored water bottles were used and were changed three times per week. CQ was dissolved in 0.9% physiological saline, filter sterilized, and administered at 45 mg/kg through either intraperitoneal or subcutaneous routes. Tumors were measured with calipers, and mice were weighed twice per week. Mice whose tumors reached 2,000 mm^3 or lost >20% body weight were killed. Between 8 and 10 mice were used for each treatment group. Statistical significance was analyzed using JMP software (SAS Institute, Inc.).

Fluorescence microscopy

For LC3 immunofluorescence staining, cells were fixed in 3% paraformaldehyde and permeabilized with 0.01% digitonin in PBS followed by a rabbit polyclonal anti-LC3 (Abgent) primary antibody detected with a cy3-conjugated anti–rabbit secondary antibody (Jackson ImmunoResearch Laboratories). Cells were imaged by using a deconvolution microscopy system (DeltaVision; Applied Precision, LLC) built on an inverted microscope (IX-70; Olympus) with a Plan Apo 60×/1.40 numerical aperture oil immersion objective lens and equipped with a filter set (Sedat Quad; Chroma Technology Corp.) with single-band excitation and emission filters, a high-resolution cooled charge-coupled device (CCD) camera (CH350; Roper Scientific), and SOFTWORX software (version 2.5; Applied Precision, LLC). For labeling of AVs with MDC, cells were incubated with 0.05 mM MDC in PBS at 37°C for 10 min and immediately analyzed by fluorescence microscopy using an inverted microscope (Eclipse TE 300; Nikon) equipped with a CCD camera (SPOT; Diagnostic Instruments, Inc.).

EM

Cells were grown to monolayer in plastic flasks and fixed in half-strength Karnovsky fixative (2% paraformaldehyde, 2.5% glutaraldehyde, 0.025% $CaCl_2$-$2H_2O$, and 0.1 M sodium cacodylate buffer, pH 7.4), and tumors were cut into small cubes (~1 mm^3) and fixed by immersion in the same fixative or in the fixative used for immuno-EM. Cells and tissues were postfixed with 1% OsO_4 and 1% $K_4Ru(II)(CN)_6$ or 1.5% $K_3Fe(CN)_6$, dehydrated in ethanol, and embedded in epon. Ultrathin sections were stained with uranyl acetate and lead citrate. All EM sections were examined with a microscope (1200EX or 1010; Jeol). AVs, i.e., autophagosomes, amphisomes, and autolysosomes, were exclusively identified by morphology. Numbers of AVs were counted on systematically sampled cytoplasmic areas of 4.5 $µm^2$ ($n \geq 64$ per condition). The percentage of AV area was measured by means of a square mesh grid laid over at least five sets of systematically sampled micrographs with each set covering a cytoplasmic area ≥80 $µm^2$. The mean percentage of apoptotic nuclei in tumor tissues was calculated from the number of apoptotic nuclei in three to four sets of 100 systematically counted tumor cell nuclei.

Immuno-EM

Small tumor blocks were fixed by immersion in 2% paraformaldehyde and 0.2% glutaraldehyde in 0.1 M phosphate buffer, pH 7.4, for 5 h at 4°C. After rinsing with PBS, the blocks were embedded in 12% gelatin, cryoprotected with 2.3 M sucrose, and frozen in liquid nitrogen. Ultrathin cryosections were cut at −120°C, picked up with 1% methylcellulose and 1.2 M sucrose, thawed, and collected on copper grids. After washing with PBS containing 0.02 M glycine, sections were incubated with rabbit anti–human LAMP1 antibodies (provided by M. Fukuda, Burnham Institute for Medical Research, La Jolla, CA; Carlsson et al., 1988) or with rat monoclonal anti–mouse LAMP1 antibody ID4B (provided by T. August, Developmental Studies Hybridoma Bank, Iowa City, IA) followed by a secondary rabbit anti–rat IgG antibody (Dako). The sections were subsequently incubated with protein A conjugated to 10-nm colloidal gold particles and contrasted with a 1.8% methylcellulose and 0.6% uranyl acetate mixture.

Cell viability and cell cycle analysis

Cell number and viability was measured using trypan blue exclusion assay using a Vi-Cell Analyzer (Beckman Coulter) or labeled with 1 µg/ml Propidium iodide (PI) in PBS/1% BSA followed by cytofluorometric analysis with a fluorescence-activated cell sorter (Becton Dickinson). FITC-conjugated annexin V was used for the assessment of phosphatidylserine exposure by fluorescence-activated cell sorter analysis. Caspase activation was analyzed using a Caspase-Glo 3/7 Assay kit (Promega). For cell cycle analysis, cells were fixed with dropwise addition of chilled 70% ethanol, washed with PBS, and resuspended in staining solution containing 50 µg/ml PI and 60 U RNase A. DNA content was analyzed by flow cytometry using the FlowJo and ModFit software (Becton Dickinson).

Multispectral imaging flow cytometry

Cells treated with various agents were stained with 1 µg/ml AO and analyzed by the ImageStream system (Amnis Corporation) using the IDEAS image analysis program. This allows quantitative characterization of single cells within a population by assessing a combination of morphology and fluorescence patterns. AO fluoresces green when bound to nuclei and red when concentrated in acidic vacuoles. The DNA AO green image and the vacuolar AO red image were first compensated into separate channels, and the percentage of apoptotic/anucleate cells (based on AO nuclear morphology and intensity) and vacuolated cells (AO red+) were quantified. Plotting AO green intensity versus the AO green bright detail area revealed three distinct populations: R2 anucleated cells (low AO green labeling and higher area caused by masking of diffuse cytoplasm), R3 apoptotic cells (intermediate to low AO green and very low AO green detail area caused by the presence of small, bright condensed nuclear fragments), and R4 live cells (intact bright nucleus). AO red intensity is plotted on the second histogram, with an arbitrary gate (R5) drawn to include events with the brightest AO red intensity.

Time-lapse video microscopy

Cells cultured in 24- or 96-well plates were imaged on an inverted microscope (IX81; Olympus; or TE300; Nikon) equipped with environmental control (37°C and 5% CO_2) and a motorized X-Y stage. Images were taken with a CCD camera (HQ2 or Cascade 512; Photometrics) at 1-h intervals with a 10× objective with phase contrast for brightfield or an FITC filter for GFP-LC3 fluorescence.

Online supplemental material

Table S1 shows a summary of Akt shRNA oligos and constructs. Table S2 shows a summary of Akt KD efficiency and effect on xenograft tumor growth for various PC3-Akt shRNA clones. Fig. S1 shows relative levels of Akt isoforms in cancer cell lines and inducible KD of Akt isoforms in U87MG cells and xenograft tumors. Fig. S2 shows the effect of GFP-targeting shRNA and Akt isoform KDs on cell cycle progression, apoptosis, and autophagy. Fig. S3 shows the effect of LAMP2, Atg7, protease inhibitors, cathepsin D siRNA, and pepstatin A on PC3 cell viability in combination with PI-103 or Akti-1/2. Fig. S4 shows CQ-promoted mitochondrial membrane depolarization and cellular ROS accumulation in combination with Akti-1/2. Fig. S5 shows NAC-rescued cell death induced by Akti + CQ. Video 1 is a time-lapse video of PC3 cells treated with DMSO control. Video 2 is a time-lapse video of PC3 cells treated with CQ alone. Video 3 is a time-lapse video of PC3 cells treated with Akti-1/2 alone. Video 4 is a time-lapse video of PC3 cells treated with both CQ and Akti-1/2. Online supplemental material is available at http://www.jcb.org/cgi/content/full/jcb.200801099/DC1.

We are grateful to R. Ohri, J. Bower, A. Arrazate, C. Byers, F. Zhong, N. Pal, S. Bheddah, J. Ramirez, I. Kasman, M. Sagolla, J. Eastham-Anderson, J. Cupp, L. Gilmour, T. George, M. Vasser, R. Scriwanek, and M. van Peski for their technical assistance, B. Gunter for statistical advice, and I. Mellman for helpful discussions and critical review of the manuscript.

All authors except A.D. Mazière, S. van Dijk, H. Wu, and J. Klumperman are employees of Genentech. This work was conducted in anticipation of the development of information appropriate for submission to the Food and Drug Administration for regulatory purposes under the Food, Drug, and Cosmetics Act.

Submitted: 18 January 2008
Accepted: 5 September 2008

References

Altomare, D.A., and J.R. Testa. 2005. Perturbations of the AKT signaling pathway in human cancer. *Oncogene.* 24:7455–7464.

Amaravadi, R., and C.B. Thompson. 2005. The survival kinases Akt and Pim as potential pharmacological targets. *J. Clin. Invest.* 115:2618–2624.

Amaravadi, R.K., D. Yu, J.J. Lum, T. Bui, M.A. Christophorou, G.I. Evan, A. Thomas-Tikhonenko, and C.B. Thompson. 2007. Autophagy inhibition enhances therapy-induced apoptosis in a Myc-induced model of lymphoma. *J. Clin. Invest.* 117:326–336.

Arico, S., A. Petiot, C. Bauvy, P.F. Dubbelhuis, A.J. Meijer, P. Codogno, and E. Ogier-Denis. 2001. The tumor suppressor PTEN positively regulates macroautophagy by inhibiting the phosphatidylinositol 3-kinase/protein kinase B pathway. *J. Biol. Chem.* 276:35243–35246.

Barnett, S.F., D. Defeo-Jones, S. Fu, P.J. Hancock, K.M. Haskell, R.E. Jones, J.A. Kahana, A.M. Kral, K. Leander, L.L. Lee, et al. 2005. Identification and characterization of pleckstrin-homology-domain-dependent and isoenzyme-specific Akt inhibitors. *Biochem. J.* 385:399–408.

Boya, P., R.A. Gonzalez-Polo, N. Casares, J.L. Perfettini, P. Dessen, N. Larochette, D. Metivier, D. Meley, S. Souquere, T. Yoshimori, et al. 2005. Inhibition of macroautophagy triggers apoptosis. *Mol. Cell. Biol.* 25:1025–1040.

Bursch, W. 2001. The autophagosomal-lysosomal compartment in programmed cell death. *Cell Death Differ.* 8:569–581.

Carew, J.S., S.T. Nawrocki, C.N. Kahue, H. Zhang, C. Yang, L. Chung, J.A. Houghton, P. Huang, F.J. Giles, and J.L. Cleveland. 2007. Targeting autophagy augments the anticancer activity of the histone deacetylase inhibitor SAHA to overcome Bcr-Abl-mediated drug resistance. *Blood.* 110:313–322.

Carlsson, S.R., J. Roth, F. Piller, and M. Fukuda. 1988. Isolation and characterization of human lysosomal membrane glycoproteins, h-lamp-1 and h-lamp-2. Major sialoglycoproteins carrying polylactosaminoglycan. *J. Biol. Chem.* 263:18911–18919.

Chen, M.L., P.Z. Xu, X.D. Peng, W.S. Chen, G. Guzman, X. Yang, A. Di Cristofano, P.P. Pandolfi, and N. Hay. 2006. The deficiency of Akt1 is sufficient to suppress tumor development in Pten+/− mice. *Genes Dev.* 20:1569–1574.

Chen, W.S., P.Z. Xu, K. Gottlob, M.L. Chen, K. Sokol, T. Shiyanova, I. Roninson, W. Weng, R. Suzuki, K. Tobe, et al. 2001. Growth retardation and increased apoptosis in mice with homozygous disruption of the Akt1 gene. *Genes Dev.* 15:2203–2208.

Cho, H., J. Mu, J.K. Kim, J.L. Thorvaldsen, Q. Chu, E.B. Crenshaw III, K.H. Kaestner, M.S. Bartolomei, G.I. Shulman, and M.J. Birnbaum. 2001a. Insulin resistance and a diabetes mellitus-like syndrome in mice lacking the protein kinase Akt2 (PKB beta). *Science.* 292:1728–1731.

Cho, H., J.L. Thorvaldsen, Q. Chu, F. Feng, and M.J. Birnbaum. 2001b. Akt1/PKBalpha is required for normal growth but dispensable for maintenance of glucose homeostasis in mice. *J. Biol. Chem.* 276:38349–38352.

de Waal, E.J., H. Vreeling-Sindelarova, J.P. Schellens, J.M. Houtkooper, and J. James. 1986. Quantitative changes in the lysosomal vacuolar system of rat hepatocytes during short-term starvation. A morphometric analysis with special reference to macro- and microautophagy. *Cell Tissue Res.* 243:641–648.

Degenhardt, K., R. Mathew, B. Beaudoin, K. Bray, D. Anderson, G. Chen, C. Mukherjee, Y. Shi, C. Gelinas, Y. Fan, et al. 2006. Autophagy promotes tumor cell survival and restricts necrosis, inflammation, and tumorigenesis. *Cancer Cell.* 10:51–64.

Downward, J. 1998. Mechanisms and consequences of activation of protein kinase B/Akt. *Curr. Opin. Cell Biol.* 10:262–267.

Dufour, G., M.J. Demers, D. Gagne, A.B. Dydensborg, I.C. Teller, V. Bouchard, I. Degongre, J.F. Beaulieu, J.Q. Cheng, N. Fujita, et al. 2004. Human intestinal epithelial cell survival and anoikis. Differentiation state-distinct regulation and roles of protein kinase B/Akt isoforms. *J. Biol. Chem.* 279:44113–44122.

Easton, R.M., H. Cho, K. Roovers, D.W. Shineman, M. Mizrahi, M.S. Forman, V.M. Lee, M. Szabolcs, R. de Jong, T. Oltersdorf, et al. 2005. Role for Akt3/protein kinase Bgamma in attainment of normal brain size. *Mol. Cell. Biol.* 25:1869–1878.

Fan, Q.W., Z.A. Knight, D.D. Goldenberg, W. Yu, K.E. Mostov, D. Stokoe, K.M. Shokat, and W.A. Weiss. 2006. A dual PI3 kinase/mTOR inhibitor reveals emergent efficacy in glioma. *Cancer Cell.* 9:341–349.

Foghsgaard, L., D. Wissing, D. Mauch, U. Lademann, L. Bastholm, M. Boes, F. Elling, M. Leist, and M. Jaattela. 2001. Cathepsin B acts as a dominant execution protease in tumor cell apoptosis induced by tumor necrosis factor. *J. Cell Biol.* 153:999–1010.

Fujiwara, K., E. Iwado, G.B. Mills, R. Sawaya, S. Kondo, and Y. Kondo. 2007. Akt inhibitor shows anticancer and radiosensitizing effects in malignant glioma cells by inducing autophagy. *Int. J. Oncol.* 31:753–760.

Gills, J.J., S. Holbeck, M. Hollingshead, S.M. Hewitt, A.P. Kozikowski, and P.A. Dennis. 2006. Spectrum of activity and molecular correlates of response to phosphatidylinositol ether lipid analogues, novel lipid-based inhibitors of Akt. *Mol. Cancer Ther.* 5:713–722.

Gonzalez-Polo, R.A., P. Boya, A.L. Pauleau, A. Jalil, N. Larochette, S. Souquere, E.L. Eskelinen, G. Pierron, P. Saftig, and G. Kroemer. 2005. The apoptosis/autophagy paradox: autophagic vacuolization before apoptotic death. *J. Cell Sci.* 118:3091–3102.

Gray, D., A.M. Jubb, D. Hogue, P. Dowd, N. Kljavin, S. Yi, W. Bai, G. Frantz, Z. Zhang, H. Koeppen, et al. 2005. Maternal embryonic leucine zipper kinase/murine protein serine-threonine kinase 38 is a promising therapeutic target for multiple cancers. *Cancer Res.* 65:9751–9761.

Gray, D.C., K.P. Hoeflich, L. Peng, Z. Gu, A. Gogineni, L.J. Murray, M. Eby, N. Kljavin, S. Seshagiri, M.J. Cole, and D.P. Davis. 2007. pHUSH: a single vector system for conditional gene expression. *BMC Biotechnol.* 7:61.

Groth-Pedersen, L., M.S. Ostenfeld, M. Hoyer-Hansen, J. Nylandsted, and M. Jaattela. 2007. Vincristine induces dramatic lysosomal changes and sensitizes cancer cells to lysosome-destabilizing siramesine. *Cancer Res.* 67:2217–2225.

Grunwald, V., L. DeGraffenried, D. Russel, W.E. Friedrichs, R.B. Ray, and M. Hidalgo. 2002. Inhibitors of mTOR reverse doxorubicin resistance conferred by PTEN status in prostate cancer cells. *Cancer Res.* 62:6141–6145.

Hoeflich, K.P., D.C. Gray, M.T. Eby, J.Y. Tien, L. Wong, J. Bower, A. Gogineni, J. Zha, M.J. Cole, H.M. Stern, et al. 2006. Oncogenic BRAF is required for tumor growth and maintenance in melanoma models. *Cancer Res.* 66:999–1006.

Irie, H.Y., R.V. Pearline, D. Grueneberg, M. Hsia, P. Ravichandran, N. Kothari, S. Natesan, and J.S. Brugge. 2005. Distinct roles of Akt1 and Akt2 in regulating cell migration and epithelial–mesenchymal transition. *J. Cell Biol.* 171:1023–1034.

Ju, X., S. Katiyar, C. Wang, M. Liu, X. Jiao, S. Li, J. Zhou, J. Turner, M.P. Lisanti, R.G. Russell, et al. 2007. Akt1 governs breast cancer progression in vivo. *Proc. Natl. Acad. Sci. USA.* 104:7438–7443.

Kanzawa, T., I.M. Germano, T. Komata, H. Ito, Y. Kondo, and S. Kondo. 2004. Role of autophagy in temozolomide-induced cytotoxicity for malignant glioma cells. *Cell Death Differ.* 11:448–457.

Kim, D., S. Kim, H. Koh, S.O. Yoon, A.S. Chung, K.S. Cho, and J. Chung. 2001. Akt/PKB promotes cancer cell invasion via increased motility and metalloproteinase production. *FASEB J.* 15:1953–1962.

Klionsky, D.J., H. Abeliovich, P. Agostinis, D.K. Agrawal, G. Aliev, D.S. Askew, M. Baba, E.H. Baehrecke, B.A. Bahr, A. Ballabio, et al. 2008. Guidelines for the use and interpretation of assays for monitoring autophagy in higher eukaryotes. *Autophagy.* 4:151–175.

Knight, Z.A., B. Gonzalez, M.E. Feldman, E.R. Zunder, D.D. Goldenberg, O. Williams, R. Loewith, D. Stokoe, A. Balla, B. Toth, et al. 2006. A pharmacological map of the PI3-K family defines a role for p110alpha in insulin signaling. *Cell.* 125:733–747.

Kroemer, G., and M. Jaattela. 2005. Lysosomes and autophagy in cell death control. *Nat. Rev. Cancer.* 5:886–897.

Levine, B., and J. Yuan. 2005. Autophagy in cell death: an innocent convict. *J. Clin. Invest.* 115:2679–2688.

Li, J., C. Yen, D. Liaw, K. Podsypanina, S. Bose, S.I. Wang, J. Puc, C. Miliaresis, L. Rodgers, R. McCombie, et al. 1997. PTEN, a putative protein tyrosine phosphatase gene mutated in human brain, breast, and prostate cancer. *Science.* 275:1943–1947.

Liaudet-Coopman, E., M. Beaujouin, D. Derocq, M. Garcia, M. Glondu-Lassis, V. Laurent-Matha, C. Prebois, H. Rochefort, and F. Vignon. 2006. Cathepsin D: newly discovered functions of a long-standing aspartic protease in cancer and apoptosis. *Cancer Lett.* 237:167–179.

Liu, X., Y. Shi, M.J. Birnbaum, K. Ye, R. De Jong, T. Oltersdorf, V.L. Giranda, and Y. Luo. 2006. Quantitative analysis of anti-apoptotic function of Akt in Akt1 and Akt2 double knock-out mouse embryonic fibroblast cells under normal and stressed conditions. *J. Biol. Chem.* 281:31380–31388.

Lockshin, R.A., and Z. Zakeri. 2004. Apoptosis, autophagy, and more. *Int. J. Biochem. Cell Biol.* 36:2405–2419.

Lum, J.J., D.E. Bauer, M. Kong, M.H. Harris, C. Li, T. Lindsten, and C.B. Thompson. 2005. Growth factor regulation of autophagy and cell survival in the absence of apoptosis. *Cell.* 120:237–248.

Maroulakou, I.G., W. Oemler, S.P. Naber, and P.N. Tsichlis. 2007. Akt1 ablation inhibits, whereas Akt2 ablation accelerates, the development of mammary adenocarcinomas in mouse mammary tumor virus (MMTV)-ErbB2/neu and MMTV-polyoma middle T transgenic mice. *Cancer Res.* 67:167–177.

Memmott, R.M., J.J. Gills, M. Hollingshead, M.C. Powers, Z. Chen, B. Kemp, A. Kozikowski, and P.A. Dennis. 2008. Phosphatidylinositol ether lipid analogues induce AMP-activated protein kinase-dependent death in LKB1-mutant non small cell lung cancer cells. *Cancer Res.* 68:580–588.

Moore, M.N., J.I. Allen, and P.J. Somerfield. 2006. Autophagy: role in surviving environmental stress. *Mar. Environ. Res.* 62:S420–S425.

Ohsumi, Y. 2001. Molecular dissection of autophagy: two ubiquitin-like systems. *Nat. Rev. Mol. Cell Biol.* 2:211–216.

Ohta, T., H. Arakawa, F. Futagami, S. Fushida, H. Kitagawa, M. Kayahara, T. Nagakawa, K. Miwa, K. Kurashima, M. Numata, et al. 1998. Bafilomycin A1 induces apoptosis in the human pancreatic cancer cell line Capan-1. *J. Pathol.* 185:324–330.

Ostenfeld, M.S., N. Fehrenbacher, M. Hoyer-Hansen, C. Thomsen, T. Farkas, and M. Jaattela. 2005. Effective tumor cell death by sigma-2 receptor ligand siramesine involves lysosomal leakage and oxidative stress. *Cancer Res.* 65:8975–8983.

Parcellier, A., L.A. Tintignac, E. Zhuravleva, and B.A. Hemmings. 2008. PKB and the mitochondria: AKTing on apoptosis. *Cell. Signal.* 1:21–30.

Peng, X.D., P.Z. Xu, M.L. Chen, A. Hahn-Windgassen, J. Skeen, J. Jacobs, D. Sundararajan, W.S. Chen, S.E. Crawford, K.G. Coleman, and N. Hay. 2003. Dwarfism, impaired skin development, skeletal muscle atrophy, delayed bone development, and impeded adipogenesis in mice lacking Akt1 and Akt2. *Genes Dev.* 17:1352–1365.

Petiot, A., E. Ogier-Denis, E.F. Blommaart, A.J. Meijer, and P. Codogno. 2000. Distinct classes of phosphatidylinositol 3′-kinases are involved in signaling pathways that control macroautophagy in HT-29 cells. *J. Biol. Chem.* 275:992–998.

Samuels, Y., and K. Ericson. 2006. Oncogenic PI3K and its role in cancer. *Curr. Opin. Oncol.* 18:77–82.

Samuels, Y., L.A. Diaz Jr., O. Schmidt-Kittler, J.M. Cummins, L. Delong, I. Cheong, C. Rago, D.L. Huso, C. Lengauer, K.W. Kinzler, et al. 2005. Mutant PIK3CA promotes cell growth and invasion of human cancer cells. *Cancer Cell.* 7:561–573.

Sarbassov, D.D., S.M. Ali, S. Sengupta, J.H. Sheen, P.P. Hsu, A.F. Bagley, A.L. Markhard, and D.M. Sabatini. 2006. Prolonged rapamycin treatment inhibits mTORC2 assembly and Akt/PKB. *Mol. Cell.* 22:159–168.

Scherz-Shouval, R., E. Shvets, E. Fass, H. Shorer, L. Gil, and Z. Elazar. 2007. Reactive oxygen species are essential for autophagy and specifically regulate the activity of Atg4. *EMBO J.* 26:1749–1760.

Seehafer, S.S., and D.A. Pearce. 2006. You say lipofuscin, we say ceroid: defining autofluorescent storage material. *Neurobiol. Aging.* 27:576–588.

Seglen, P.O., and P.B. Gordon. 1982. 3-Methyladenine: specific inhibitor of autophagic/lysosomal protein degradation in isolated rat hepatocytes. *Proc. Natl. Acad. Sci. USA.* 79:1889–1892.

Shoemaker, J.P., and R.K. Dagher. 1979. Remissions of mammary adenocarcinoma in hypothyroid mice given 5-fluorouracil and chloroquine phosphate. *J. Natl. Cancer Inst.* 62:1575–1578.

Skeen, J.E., P.T. Bhaskar, C.C. Chen, W.S. Chen, X.D. Peng, V. Nogueira, A. Hahn-Windgassen, H. Kiyokawa, and N. Hay. 2006. Akt deficiency impairs normal cell proliferation and suppresses oncogenesis in a p53-independent and mTORC1-dependent manner. *Cancer Cell.* 10:269–280.

Stahl, J.M., A. Sharma, M. Cheung, M. Zimmerman, J.Q. Cheng, M.W. Bosenberg, M. Kester, L. Sandirasegarane, and G.P. Robertson. 2004. Deregulated Akt3 activity promotes development of malignant melanoma. *Cancer Res.* 64:7002–7010.

Stambolic, V., and J.R. Woodgett. 2006. Functional distinctions of protein kinase B/Akt isoforms defined by their influence on cell migration. *Trends Cell Biol.* 16:461–466.

Sun, H., R. Lesche, D.M. Li, J. Liliental, H. Zhang, J. Gao, N. Gavrilova, B. Mueller, X. Liu, and H. Wu. 1999. PTEN modulates cell cycle progression and cell survival by regulating phosphatidylinositol 3,4,5,-trisphosphate and Akt/protein kinase B signaling pathway. *Proc. Natl. Acad. Sci. USA.* 96:6199–6204.

Takeuchi, H., Y. Kondo, K. Fujiwara, T. Kanzawa, H. Aoki, G.B. Mills, and S. Kondo. 2005. Synergistic augmentation of rapamycin-induced autophagy in malignant glioma cells by phosphatidylinositol 3-kinase/protein kinase B inhibitors. *Cancer Res.* 65:3336–3346.

Tanno, S., S. Tanno, Y. Mitsuuchi, D.A. Altomare, G.H. Xiao, and J.R. Testa. 2001. AKT activation up-regulates insulin-like growth factor I receptor expression and promotes invasiveness of human pancreatic cancer cells. *Cancer Res.* 61:589–593.

Terman, A., B. Gustafsson, and U.T. Brunk. 2006. The lysosomal-mitochondrial axis theory of postmitotic aging and cell death. *Chem. Biol. Interact.* 163:29–37.

Tschopp, O., Z.Z. Yang, D. Brodbeck, B.A. Dummler, M. Hemmings-Mieszczak, T. Watanabe, T. Michaelis, J. Frahm, and B.A. Hemmings. 2005. Essential role of protein kinase B gamma (PKB gamma/Akt3) in postnatal brain development but not in glucose homeostasis. *Development.* 132:2943–2954.

Yamamoto, A., Y. Tagawa, T. Yoshimori, Y. Moriyama, R. Masaki, and Y. Tashiro. 1998. Bafilomycin A1 prevents maturation of autophagic vacuoles by inhibiting fusion between autophagosomes and lysosomes in rat hepatoma cell line, H-4-II-E cells. *Cell Struct. Funct.* 23:33–42.

Yang, Z.Z., O. Tschopp, N. Di-Poi, E. Bruder, A. Baudry, B. Dummler, W. Wahli, and B.A. Hemmings. 2005. Dosage-dependent effects of Akt1/protein kinase Balpha (PKBalpha) and Akt3/PKBgamma on thymus, skin, and cardiovascular and nervous system development in mice. *Mol. Cell. Biol.* 25:10407–10418.

Yoeli-Lerner, M., G.K. Yiu, I. Rabinovitz, P. Erhardt, S. Jauliac, and A. Toker. 2005. Akt blocks breast cancer cell motility and invasion through the transcription factor NFAT. *Mol. Cell.* 20:539–550.

Yousefi, S., R. Perozzo, I. Schmid, A. Ziemiecki, T. Schaffner, L. Scapozza, T. Brunner, and H.U. Simon. 2006. Calpain-mediated cleavage of Atg5 switches autophagy to apoptosis. *Nat. Cell Biol.* 8:1124–1132.

Yu, L., F. Wan, S. Dutta, S. Welsh, Z. Liu, E. Freundt, E.H. Baehrecke, and M. Lenardo. 2006. Autophagic programmed cell death by selective catalase degradation. *Proc. Natl. Acad. Sci. USA.* 103:4952–4957.

Zhao, J., J.J. Brault, A. Schild, and A.L. Goldberg. 2008. Coordinate activation of autophagy and the proteasome pathway by foxO transcription factor. *Autophagy.* 4:378–380.